ESTADO DE ESFUERZOS EN EL SUR Y NORTE DE HONDURAS

Allan López

Centro de Investigaciones en Ciencias Geológicas
Universidad de Costa Rica

Ingeniería Civil
Universidad Latina de Costa Rica

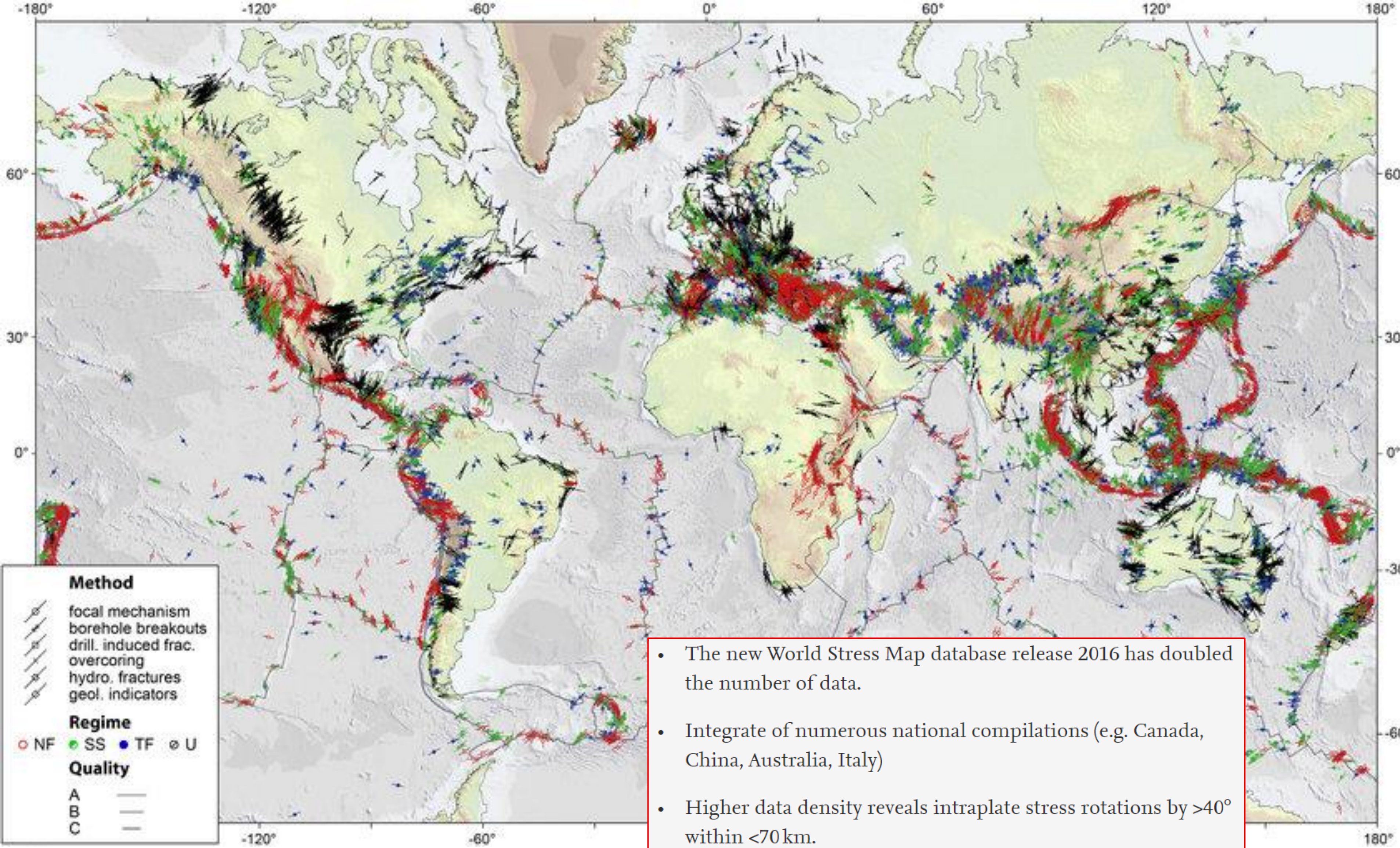

- The new World Stress Map database release 2016 has doubled the number of data.
- Integrate of numerous national compilations (e.g. Canada, China, Australia, Italy)
- Higher data density reveals intraplate stress rotations by >40° within <70 km.
- Absolute plate motion is often not the control of intraplate stress orientation.

The WSM database release 2016 contains 42,870 data records within the upper 40 km of the Earth’s crust

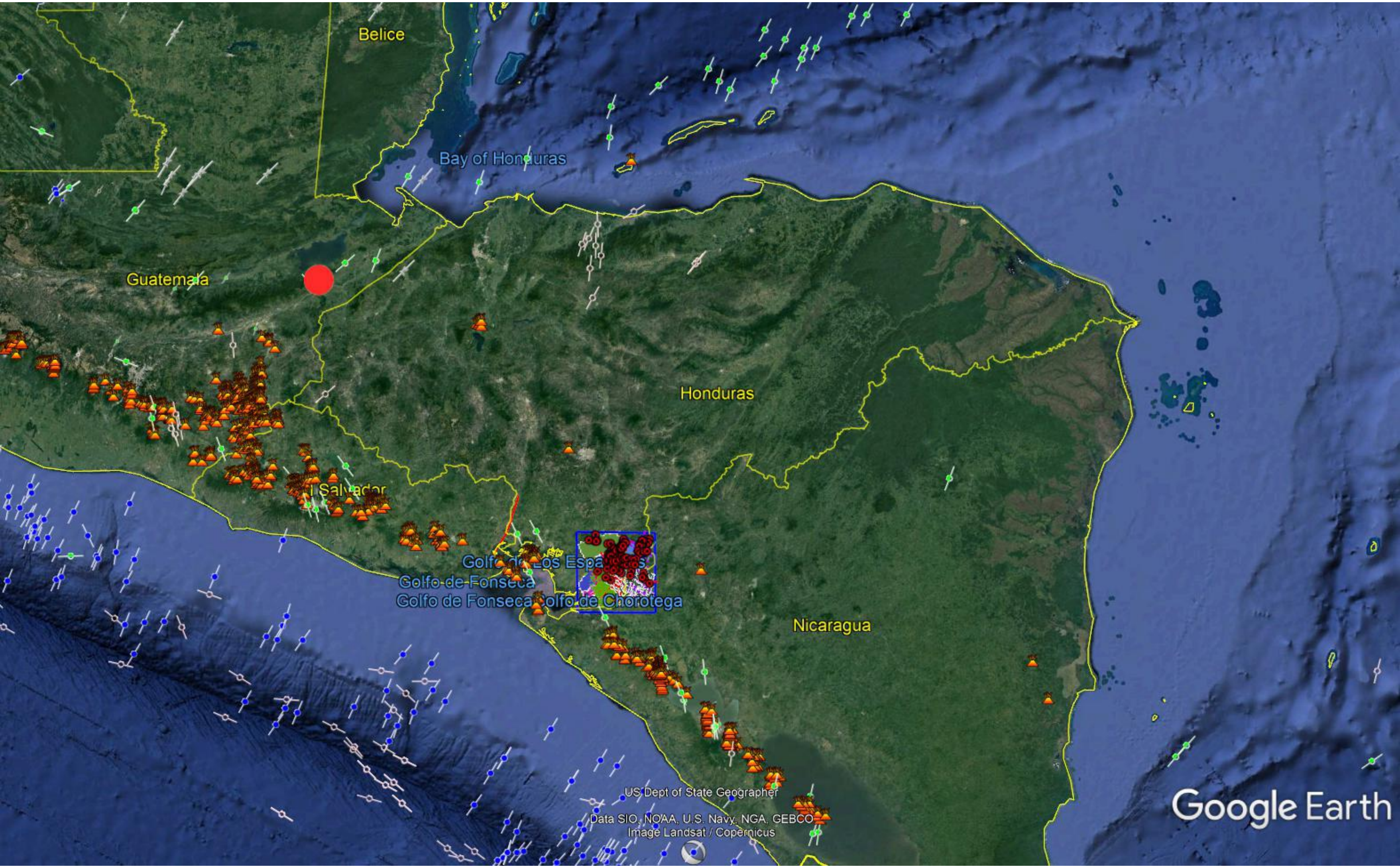
Belice
Bay of Honduras
Guatemala
Honduras
Salvador
Golfo de Los Españoles
Golfo de Fonseca
Golfo de Fonseca
Golfo de Chorotega
Nicaragua
US Dept of State Geographer
Data SIO, NOAA, U.S. Navy, NGA, GEBCO
Image Landsat / Copernicus
Google Earth

El conocimiento de las características y propiedades físicas y mecánicas del ***estado de esfuerzo tectónico*** prevaleciente en la corteza terrestre es de fundamental importancia para la sociedad y la industria, ya que tiene implicaciones y aplicaciones directas en:

- La caracterización de reservorios geotérmicos, de petróleo, gas y su administración racional y segura.

- La estabilidad de minas, túneles carreteros y de conducción de agua, vertederos de desechos tóxicos y no tóxicos.
  En general para las obras subterráneas.

- Calibración de modelos numéricos geo-mecánicos.

- Simulaciones termo, hidromecánicas en 4D.

- Evaluación del peligro y amenaza sísmica, mediante el análisis de la ***Tendencia al deslizamiento de la falla y el potencial de fractura.***

- Mecánismos focales de terremotos
- Elongaciones-breakouts en pozos y fracturas inducidas por la perforación
- Medidas In-situ (overcoring, fracturación hidráulica, borehole slotter)
- Datos Geólogicos recientes (análisis de fallas mesoscópicas y alineamiento de conos y diques volcánicos Cuaternarios)

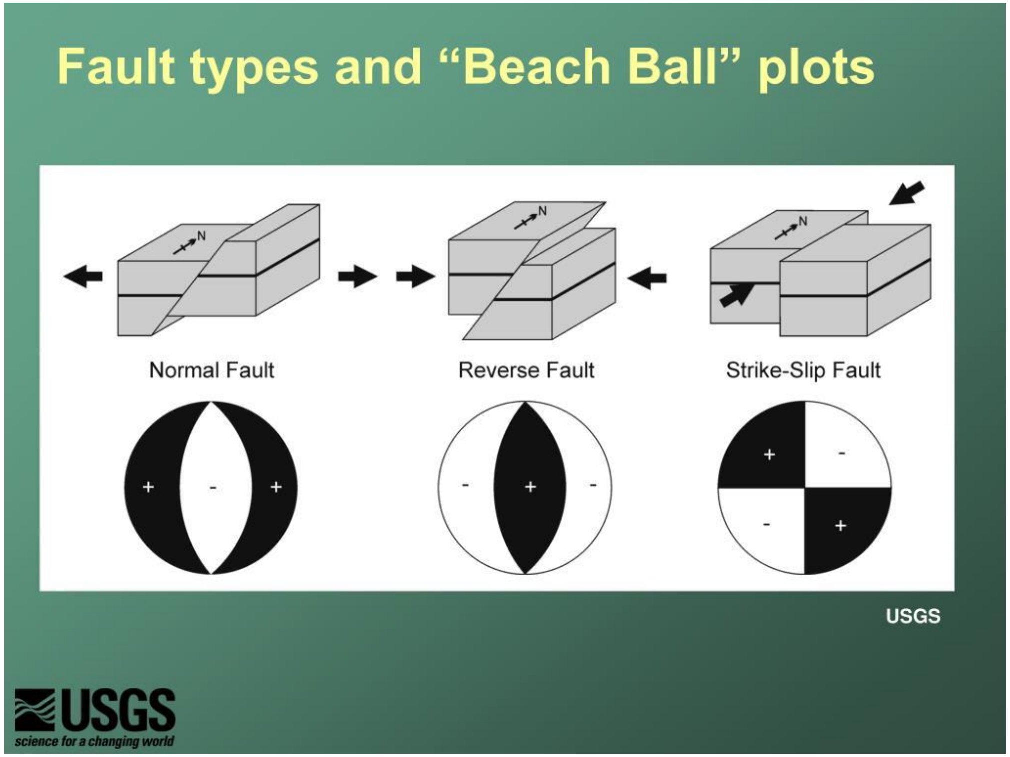

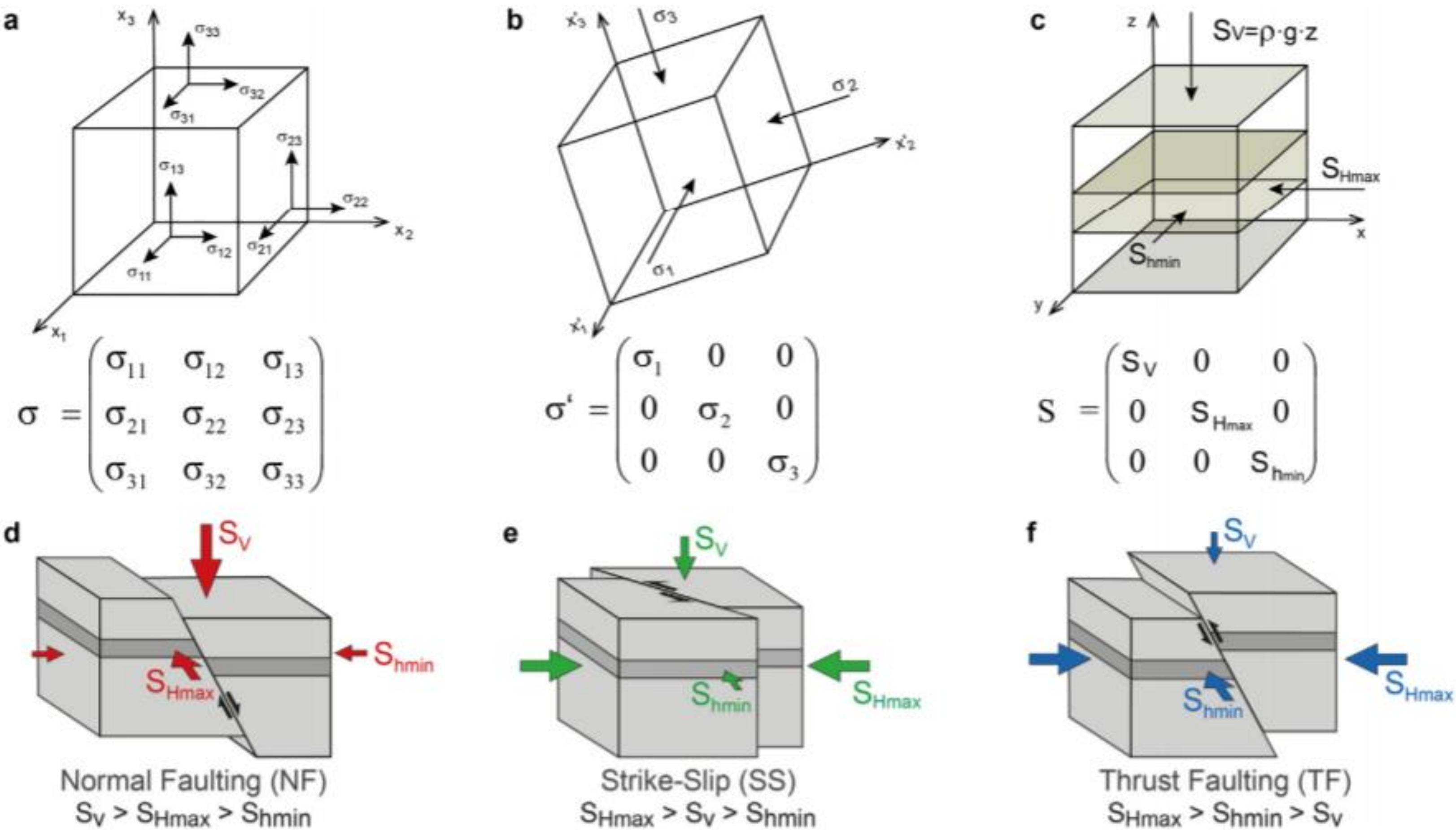

Fig. 1. a) The components of the stress tensor define the stress state at a point and enable to compute the stress vector on any surface within a body. To describe the stress tensor components an infinitely small cube with unit surfaces is used. The forces acting on the cube faces can be decomposed in forces acting parallel and those acting normal to the surface. The first create the normal stress components, the second create the shear stress components of the stress tensor. b) Due to the conservation of momentum the stress tensor has to be symmetric. This implies that a coordinate system exists where shear stresses vanish along the faces of the cube. In this principal axis system the remaining three stresses are the principal stresses. c) Assuming that the vertical stress in the Earth crust $S_V = g{\cdot}\rho{\cdot}z$ is a principal stress (g is gravitational acceleration, ρ is the rock density, z the depth), the two horizontal stresses S_{hmin} and S_{Hmax}, the minimum and maximum horizontal stress, respectively, are principal stresses as well. This so-called reduced stress tensor is fully determined with four components: the S_{Hmax} orientation and the magnitudes of S_V, S_{Hmax} and S_{hmin}. The stress information provided in the WSM database is for all data records the S_{Hmax} orientation and for most data records the stress regime which indicates the relative stress magnitudes. d) Normal faulting stress regime where S_V is larger than the horizontal stresses ($S_V = \sigma_1$). e) Strike-slip faulting stress regime where S_V is the intermediate principal stress ($S_V = \sigma_2$). f) Thrust faulting stress regime where S_V is smaller than the horizontal stresses ($S_V = \sigma_3$).

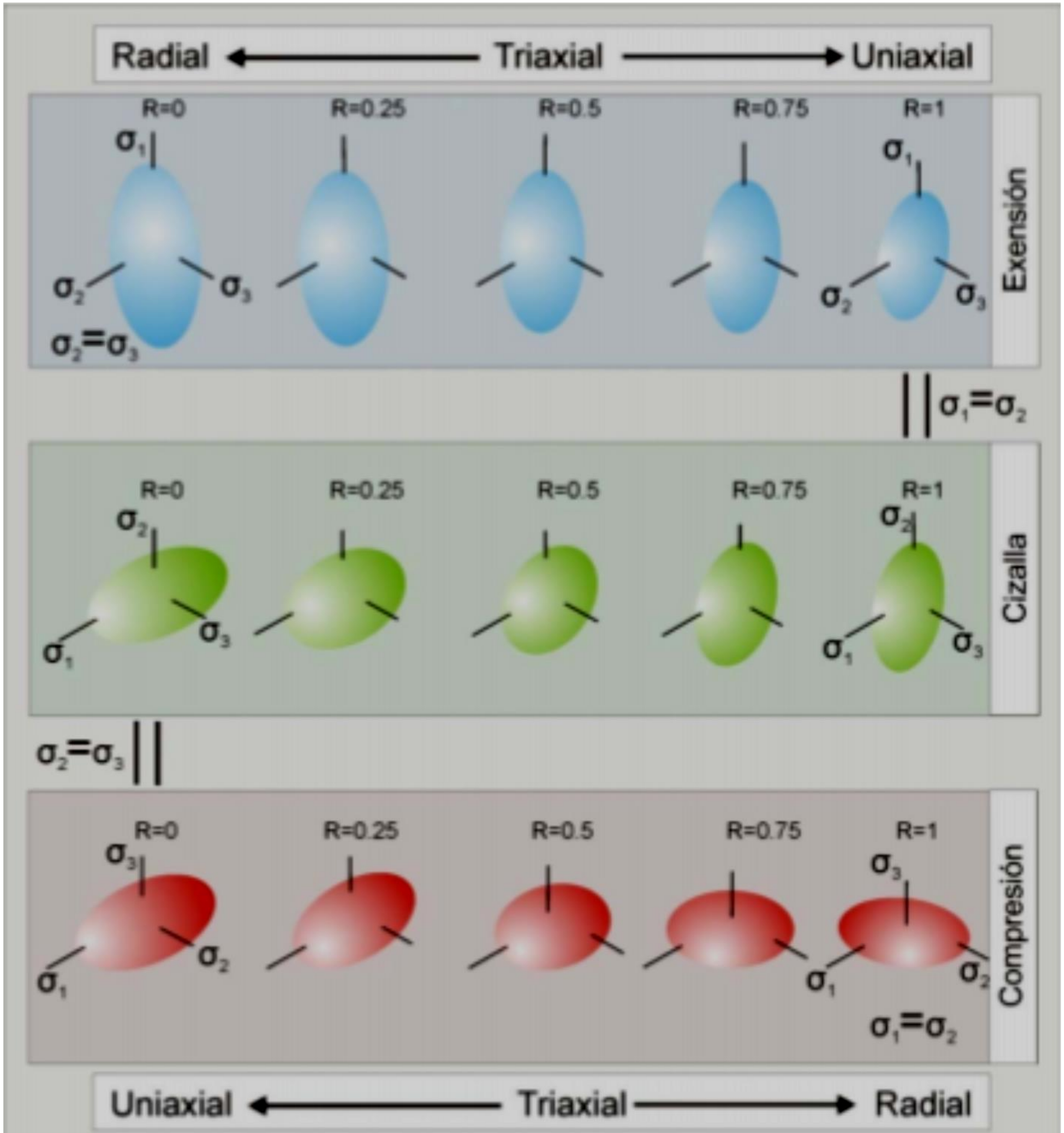

Radial
Triaxial
Uniaxial
R=0
R=0.25
R=0.5
R=0.75
R=1
σ_1
σ_2
σ_3
$\sigma_2=\sigma_3$
Exensión
$\sigma_1=\sigma_2$
Cizalla
$\sigma_2=\sigma_3$
Compresión
$\sigma_1=\sigma_2$
Uniaxial
Triaxial
Radial

El problema inverso en los esfuerzos tectónicos

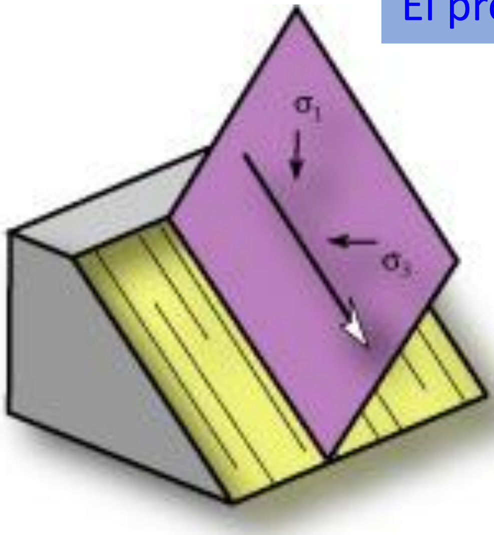

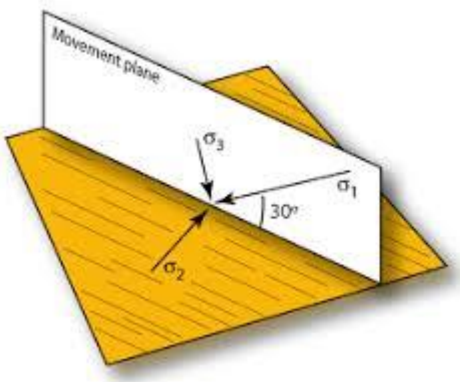

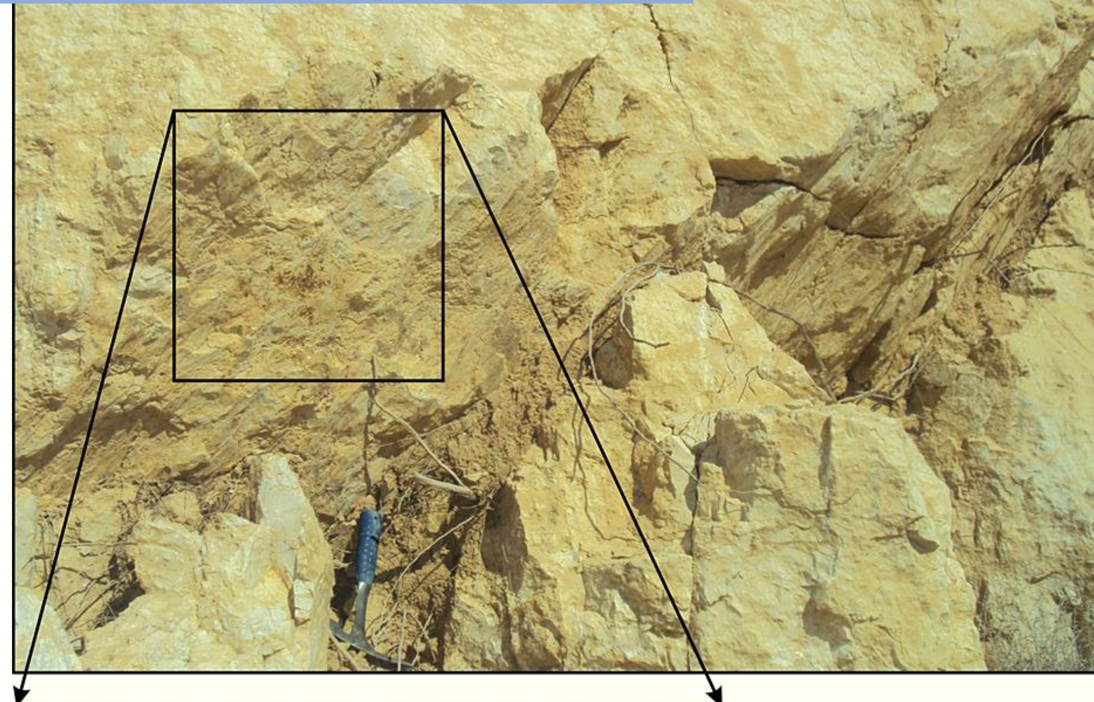

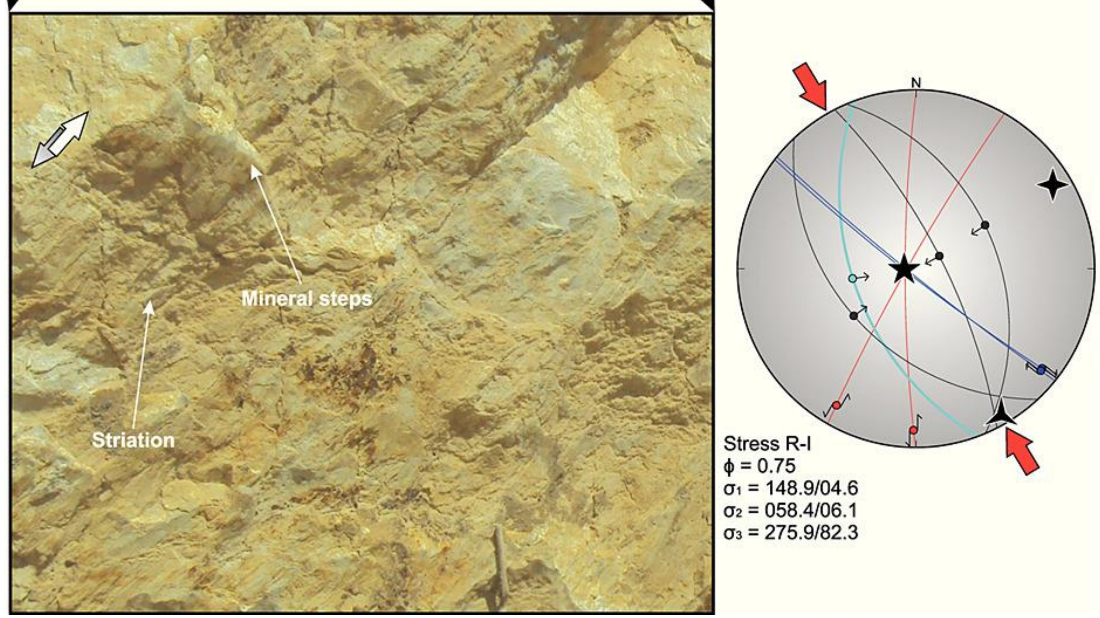

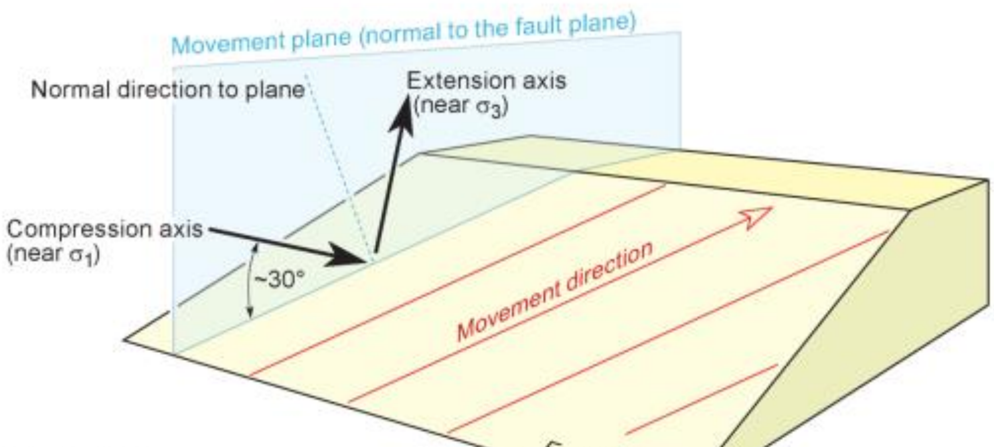

Theoretical
compression and extension axes of a fault

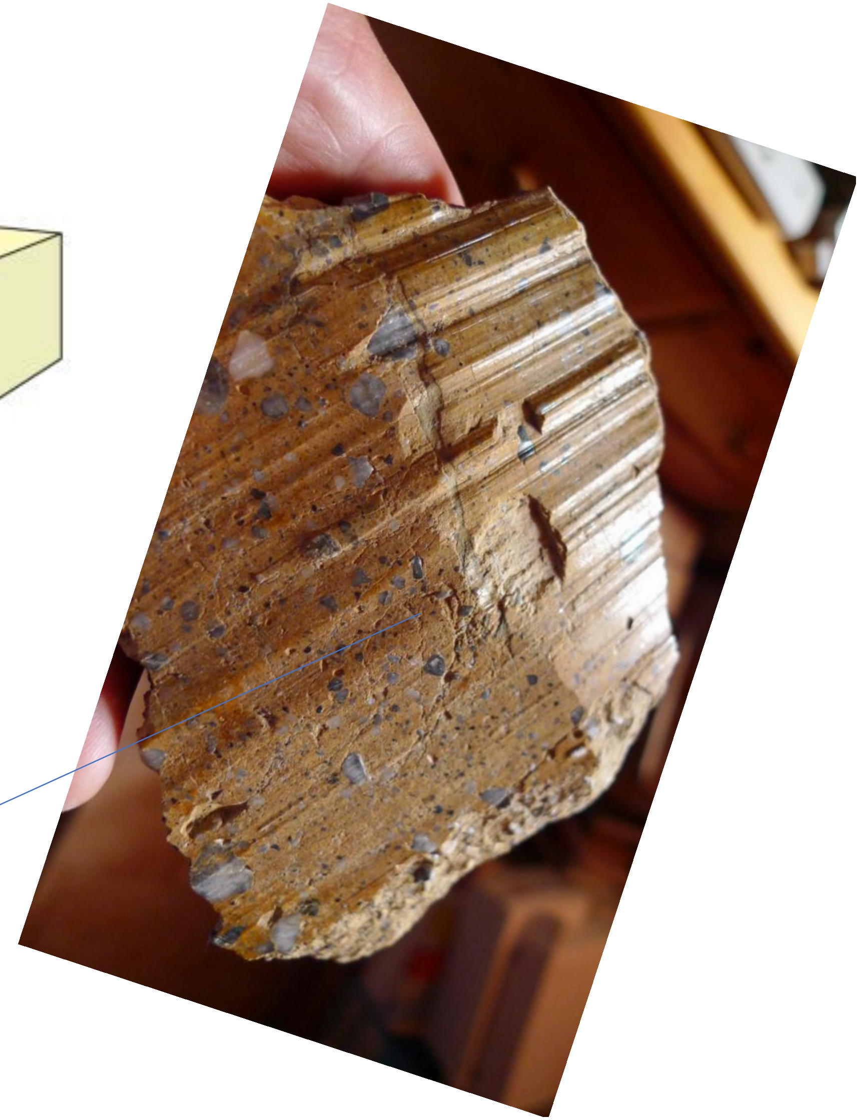

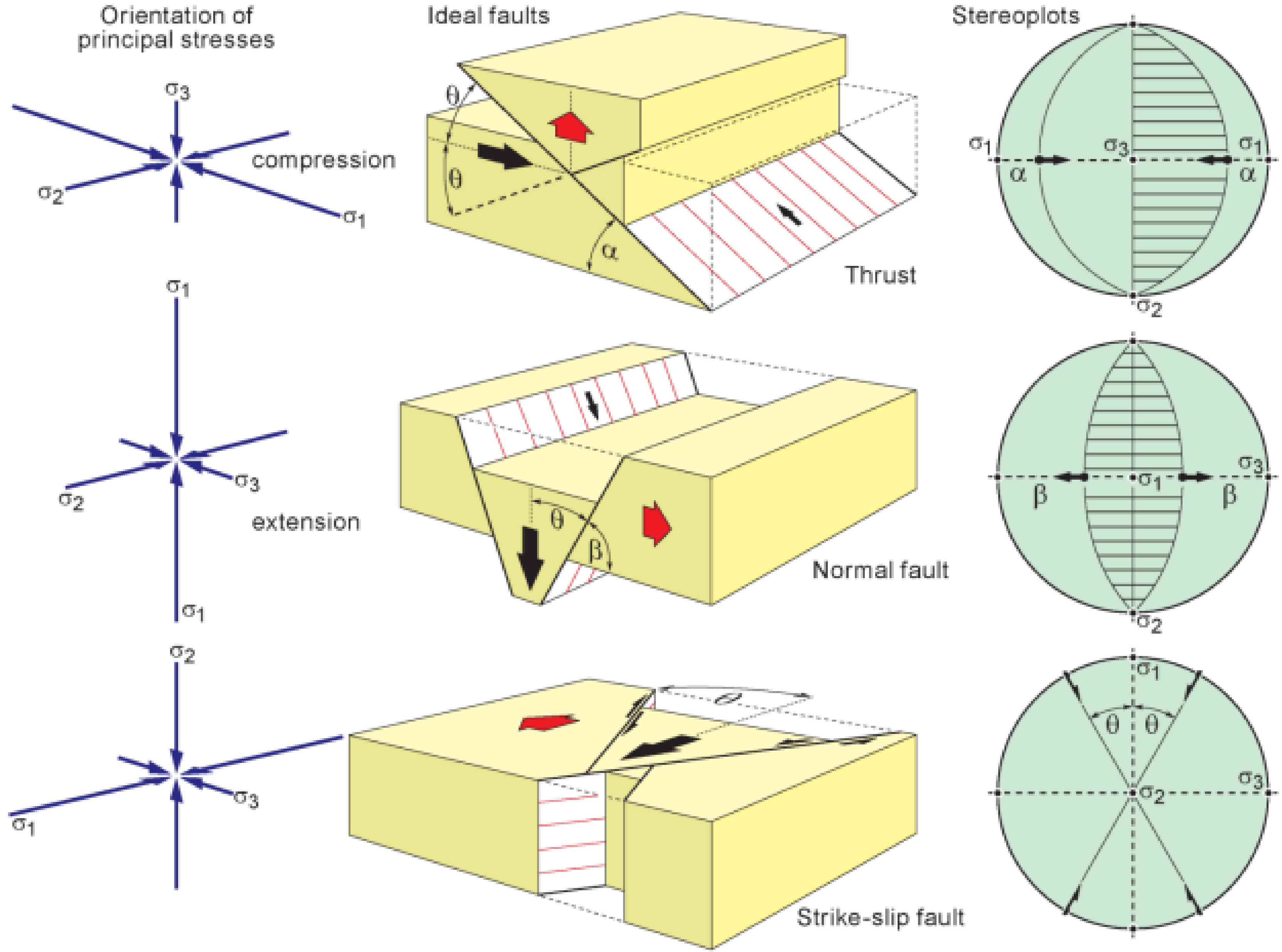

Dynamic interpretation of faults: Anderson's "standard" relationship between stresses and ideal faults

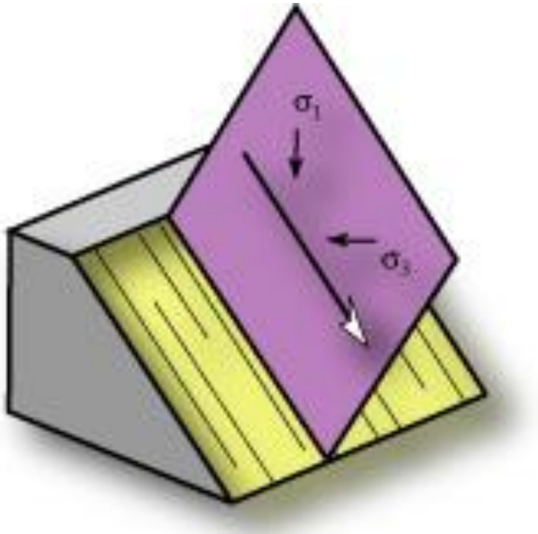

σ1
σ3

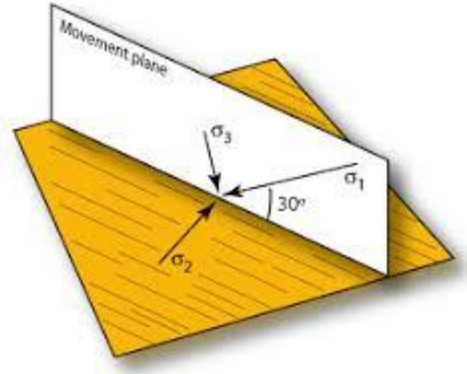

Movement plane
σ3
σ1
30°
σ2

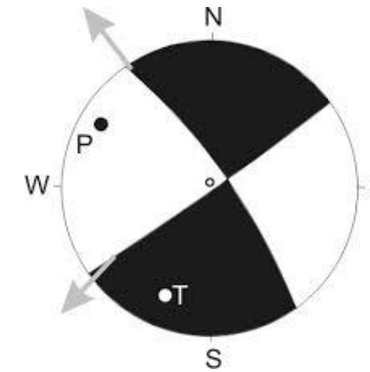

N
P
W
E
T
S

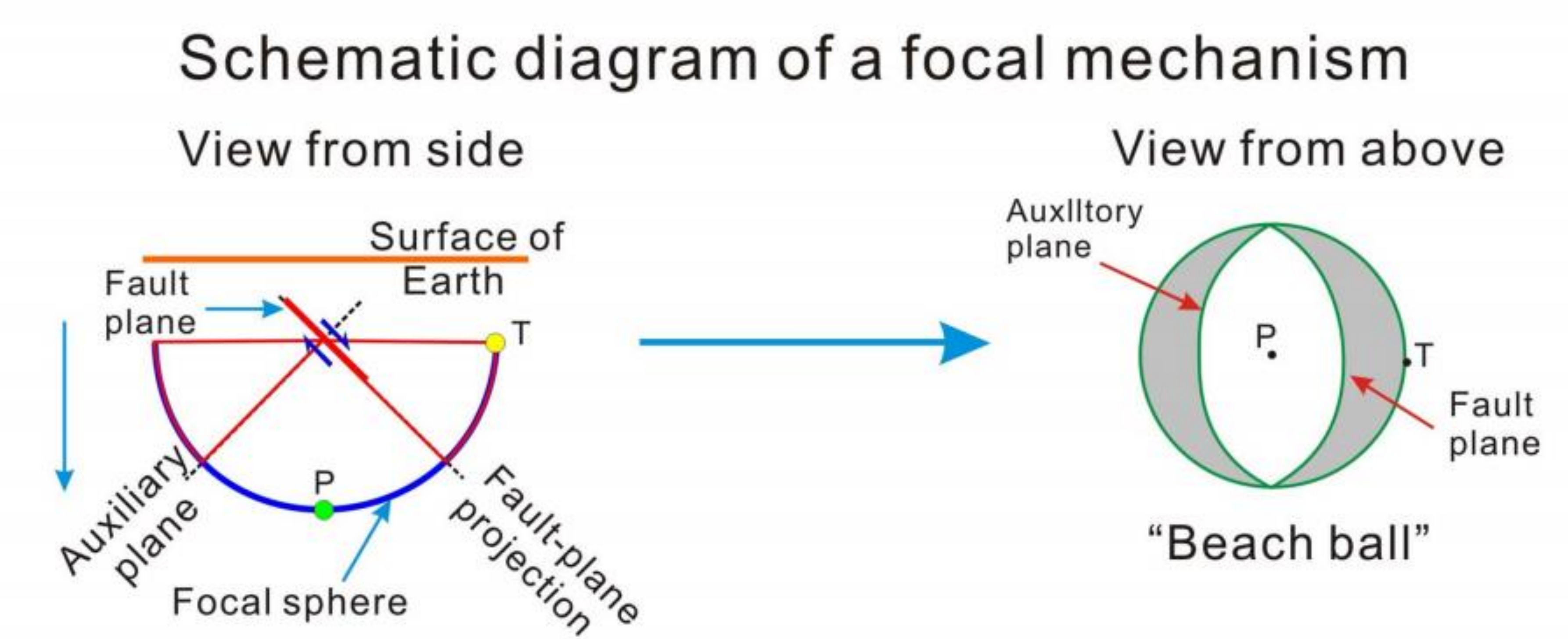

Schematic diagram of a focal mechanism
View from side
View from above
Surface of Earth
Fault plane
T
Auxiliary plane
P
Focal sphere
Fault-plane projection
Auxlltory plane
P
T
Fault plane
"Beach ball"

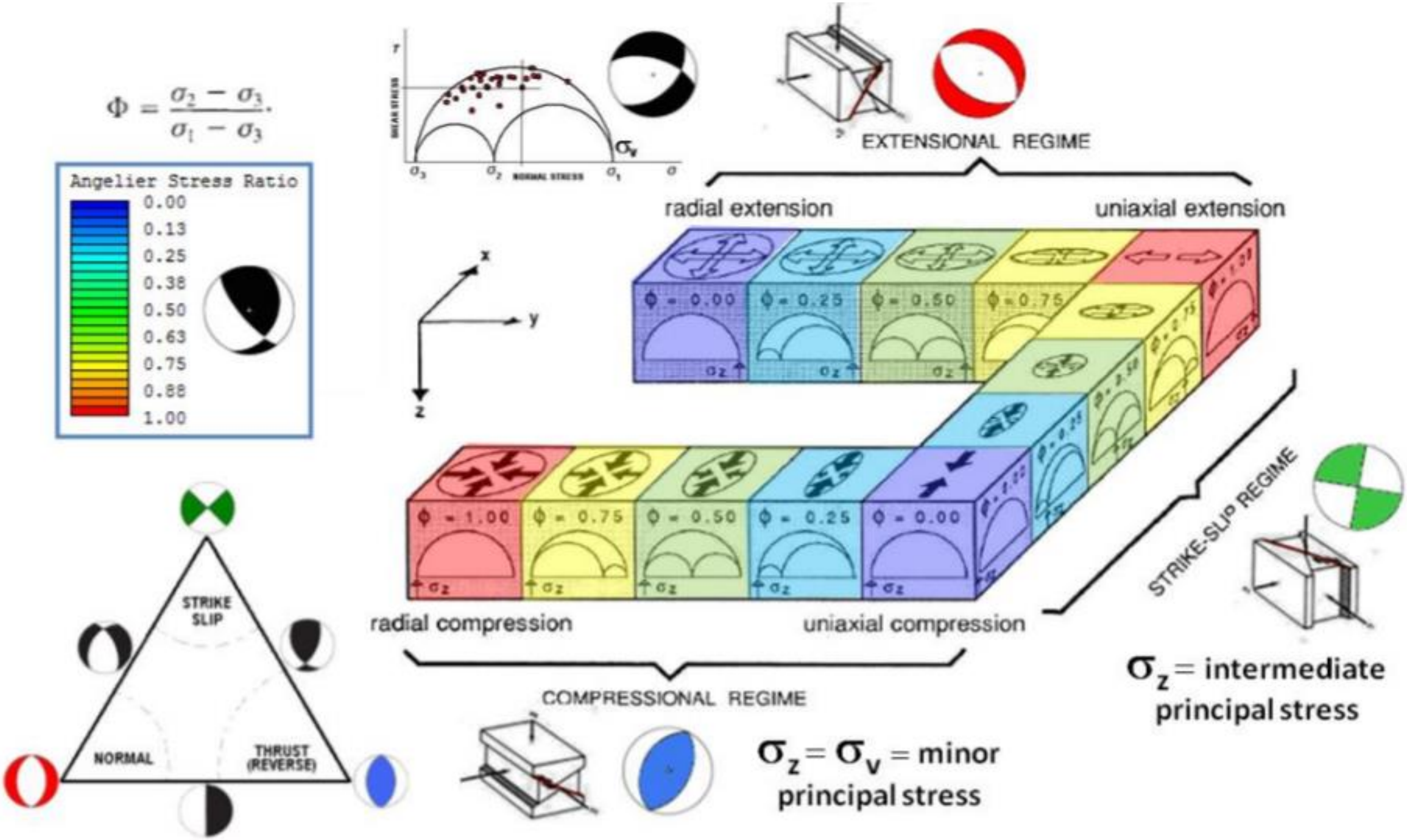

Figure 9 Classification of different tectonic stress states for different Fault geometries as plotted from beachballs and ternary diagrams, after Carter (2015b) (with key inset diagram modified from original created by Ritz 1994)

Por eso, NO hay que decir esta falla es normal, inversa, de rumbo, sino . . .
el último movimiento conocido es …. (y en el futuro puede reactivarse con otra cinemática)

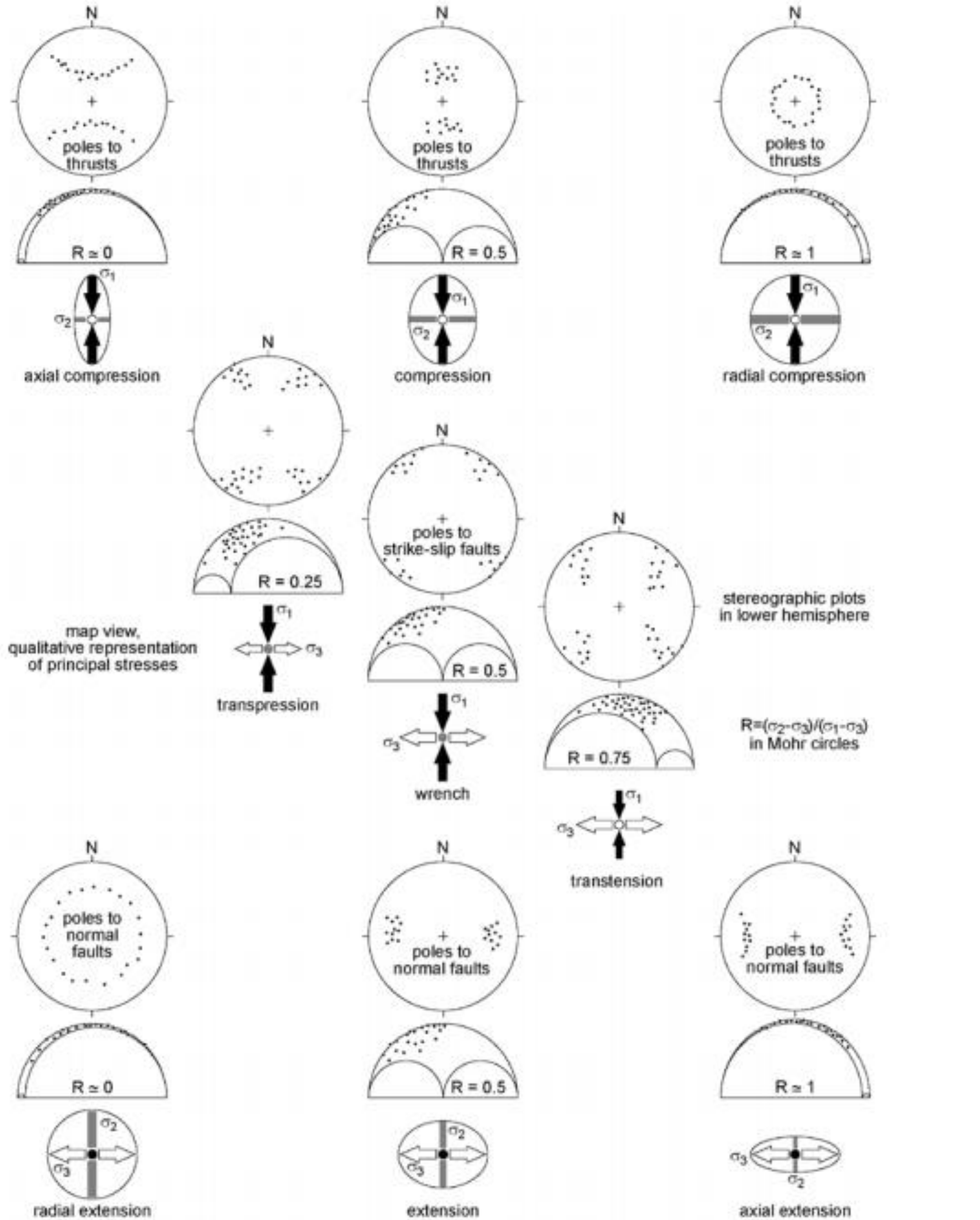

Tectonic regimes defined by paleostress calculations

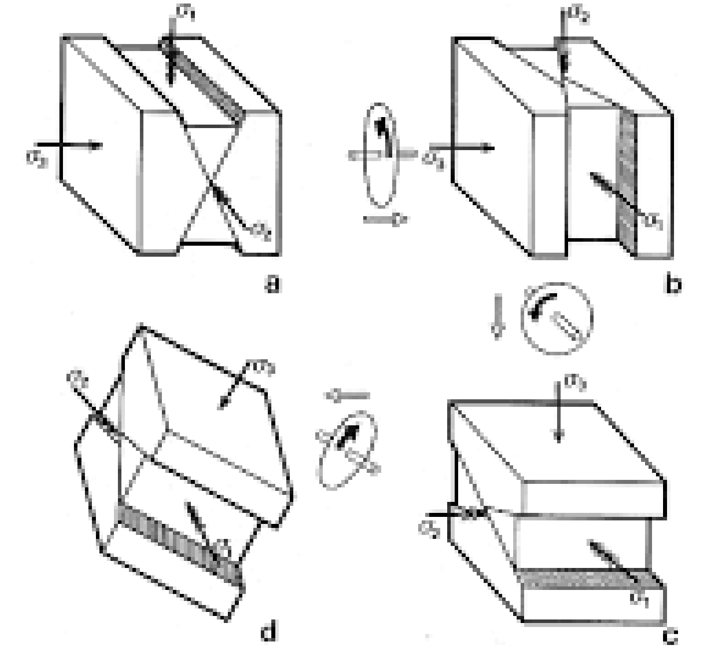

Fig. 4.18. Conjugate fault patterns. (a) Conjugate normal dip-slip faults. (b) Conjugate strike-slip faults. (c) Conjugate reverse dip-slip faults. (d) Conjugate oblique-slip faults. Principal stress axes shown with triple, double and single arrow-heads (σ_1, σ_2 and σ_3, respectively). Wheels with black arrows indicate rotations necessary to obtain (b) from (a), (c) from (b), and (d) from (c). Each of the first two rotations equals 90°.

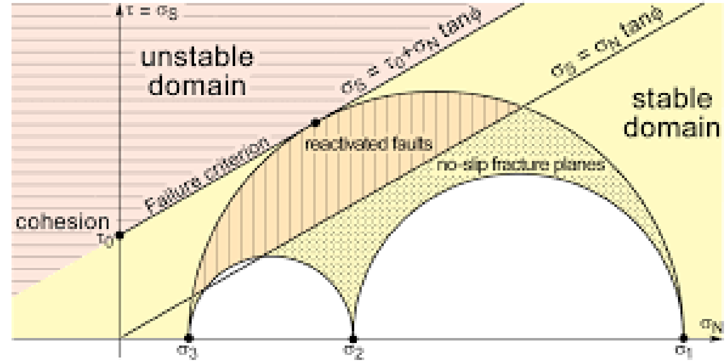

Domain of reactivated, inherited fractures
in a Mohr diagram with the three principal stresses

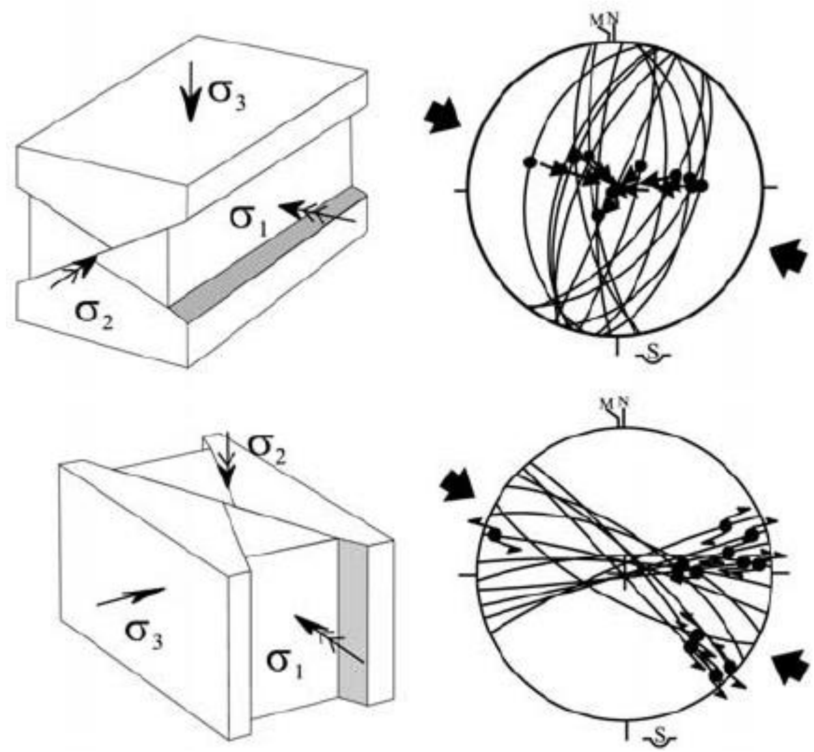

Por eso, NO hay que decir esta falla es normal, inversa, de rumbo, sino . . .
el último movimiento conocido es …. (y en el futuro puede reactivarse con otra cinemática)

Permutación de ejes

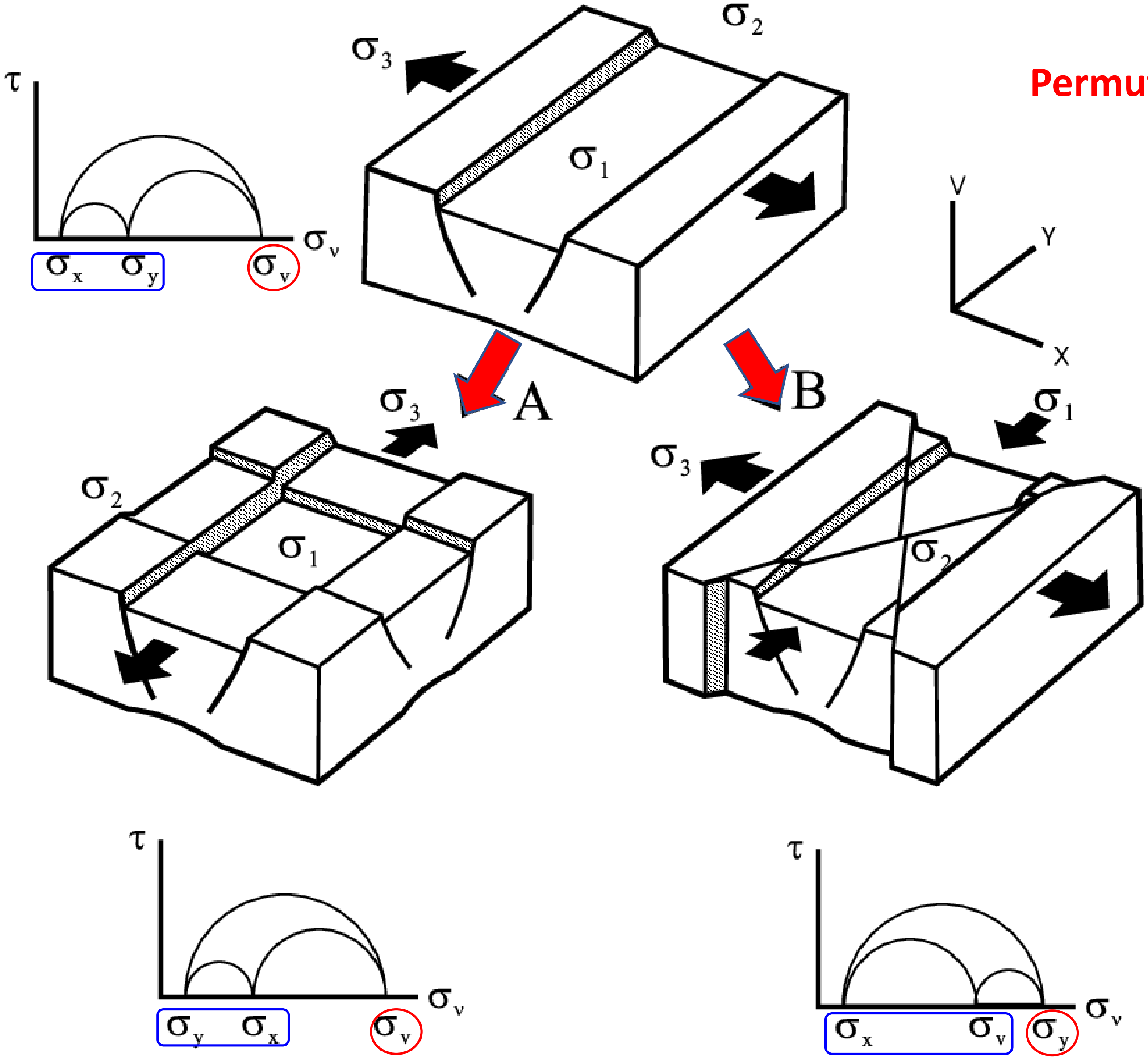

Por eso, NO hay que decir esta falla es normal, inversa, de rumbo, sino . . .
el último movimiento conocido es …. (y en el futuro puede reactivarse con otra cinemática)

ESTADO DE ESFUERZOS EN EL SUR Y NORTE DE HONDURAS

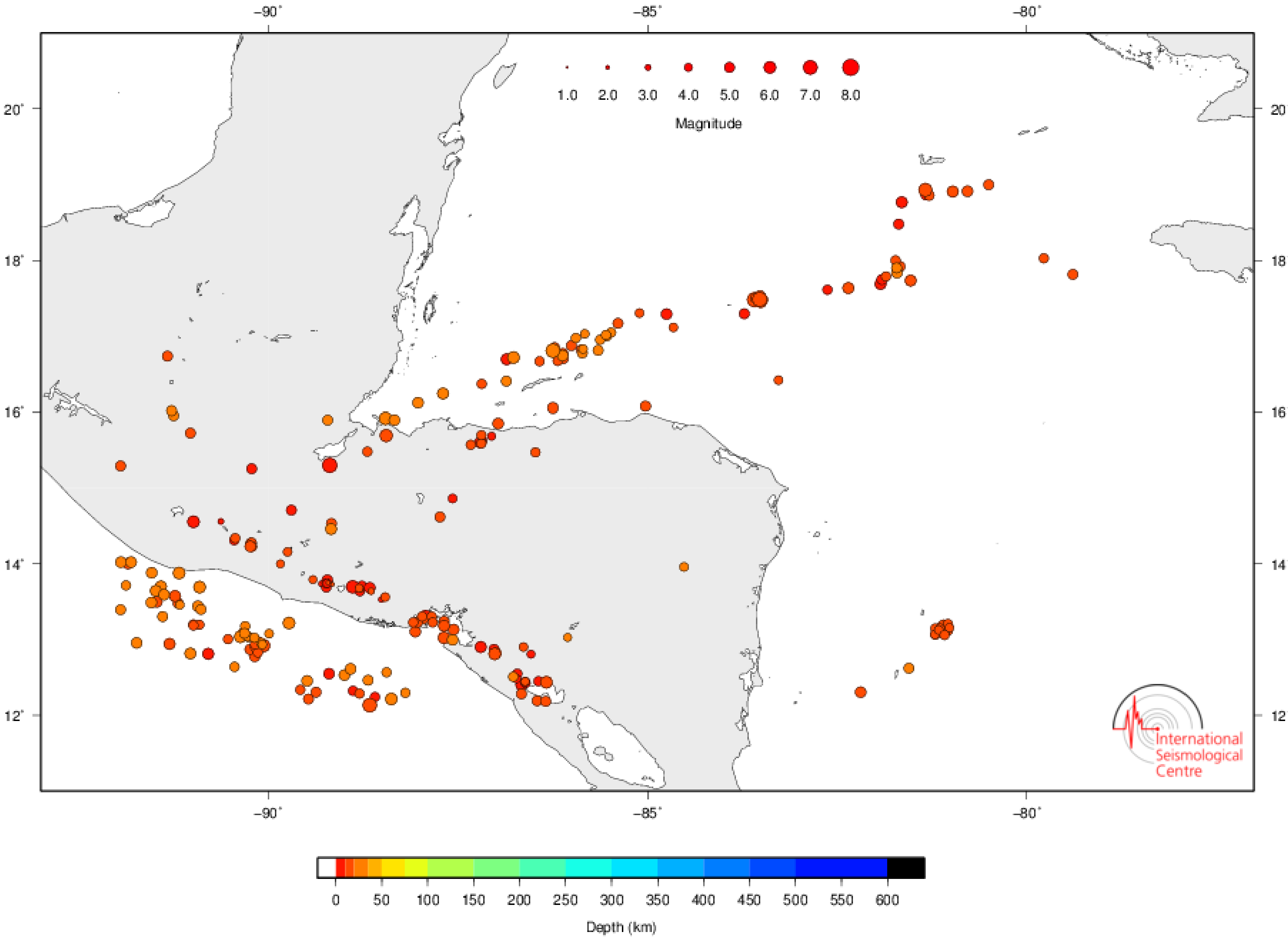

http://www.isc.ac.uk/cgi-bin/makegmtmap?userid=2374455&region=270/281.17/12.12/20.18

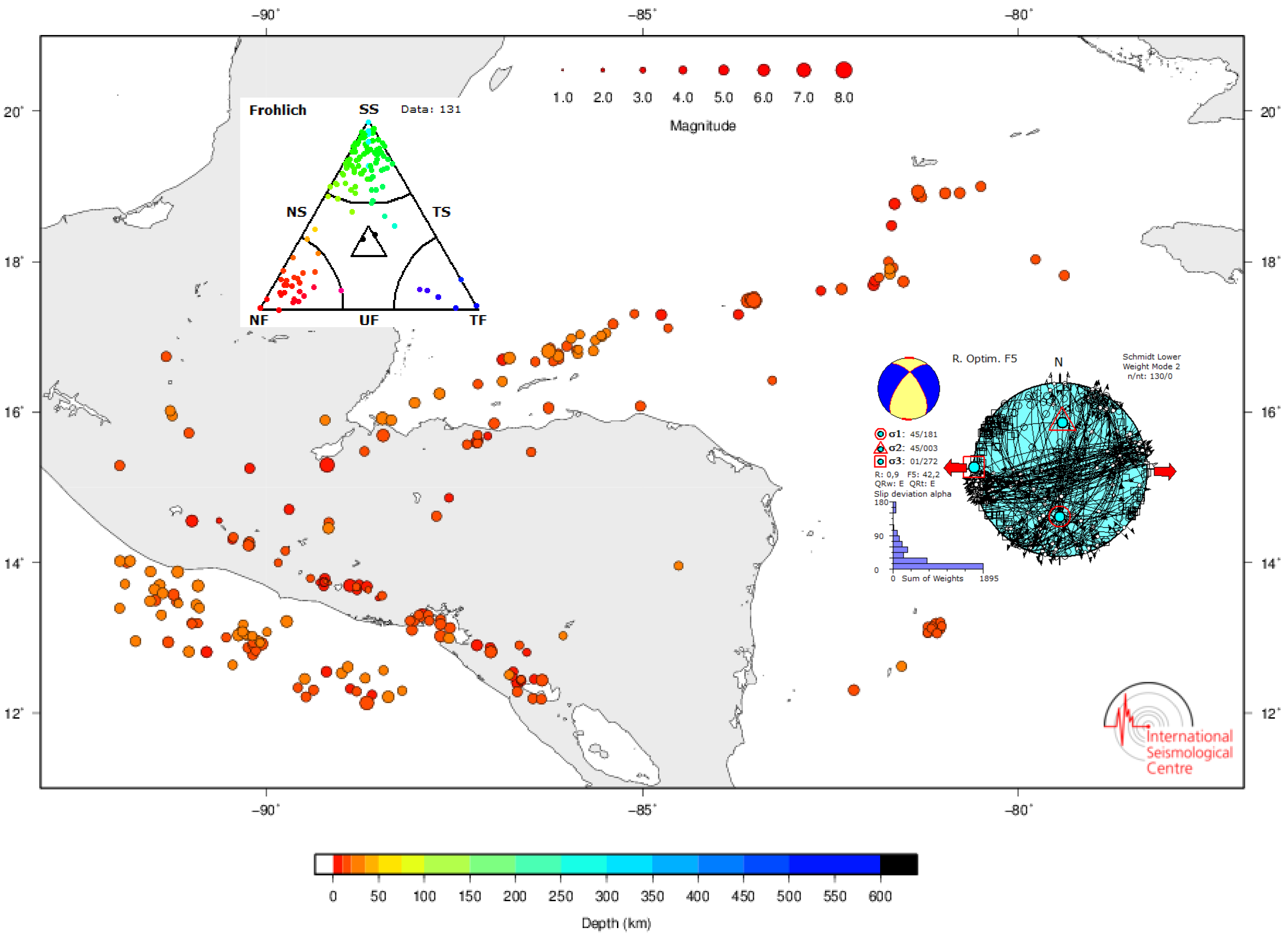

http://www.isc.ac.uk/cgi-bin/makegmtmap?userid=2374455&region=270/281.17/12.12/20.18

Mecanismos focales regionales CMT
Escena en GeoMapApp

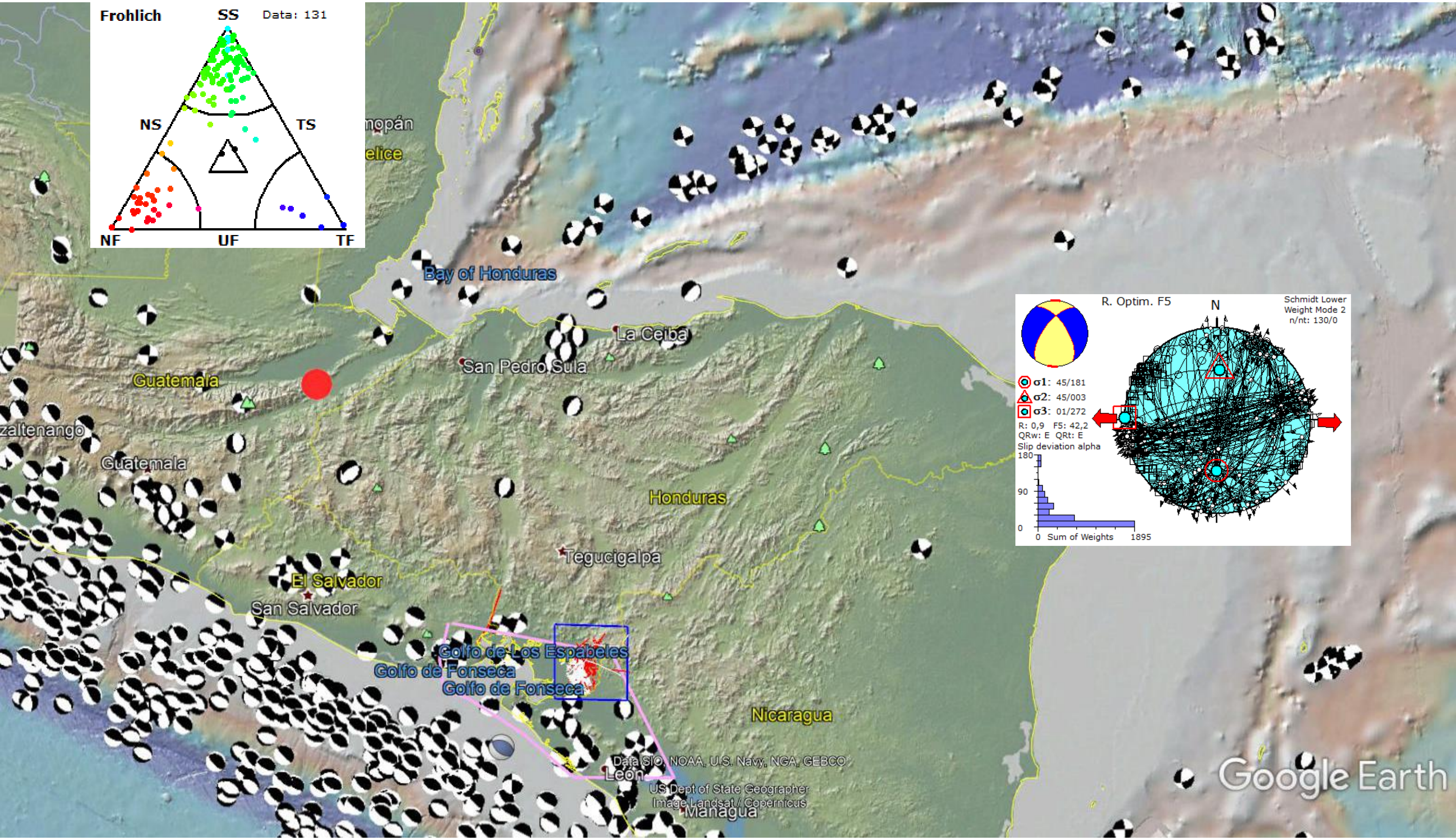

1 Plano nodal de cada evento Mw > 4.0

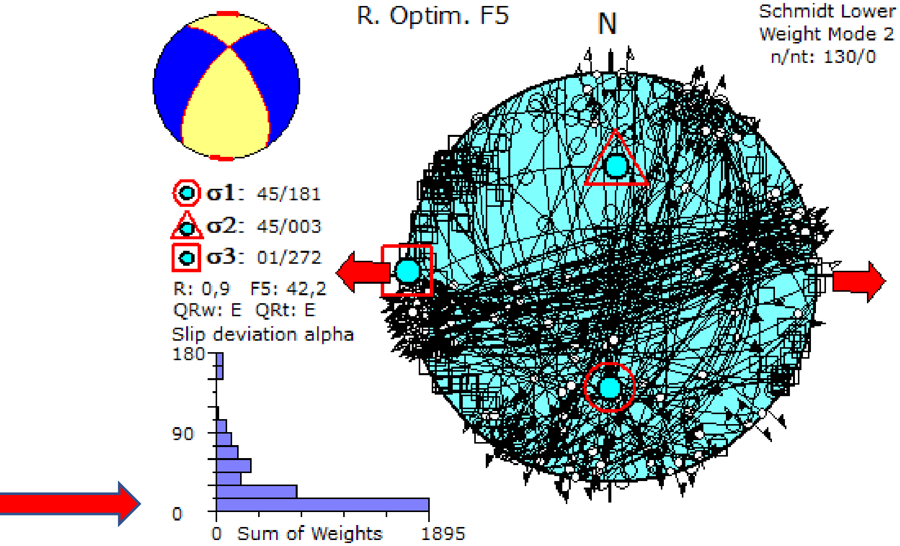

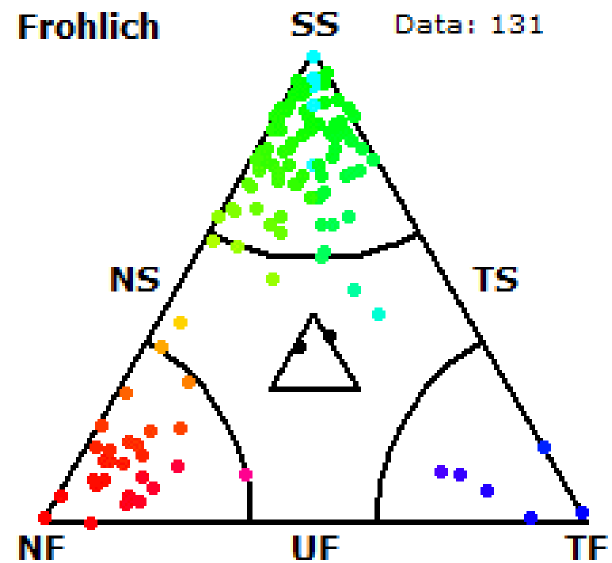

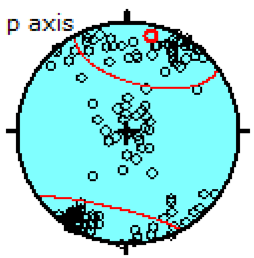

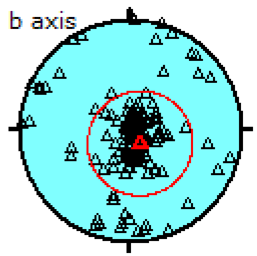

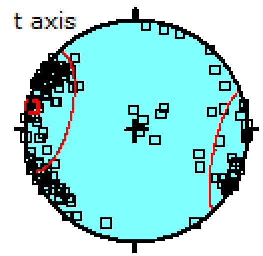

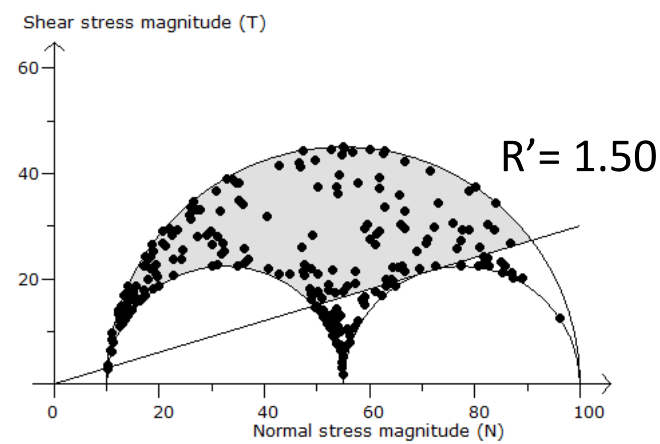

2 Planos nodales de cada evento Mw > 4.0

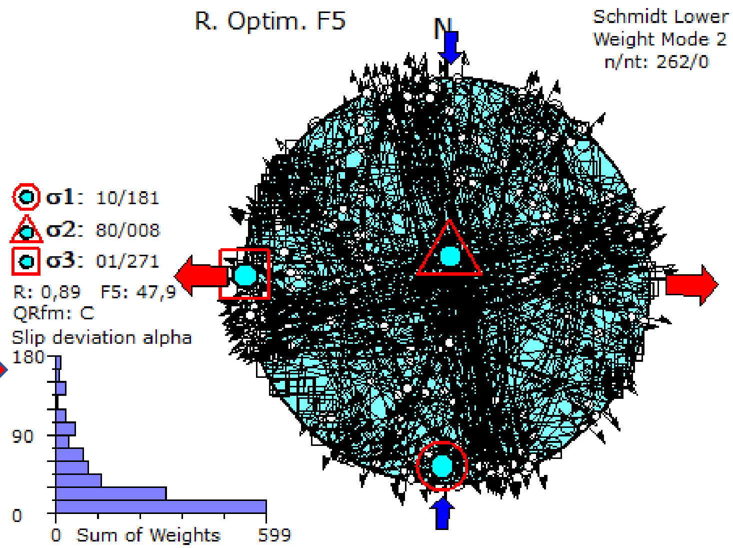

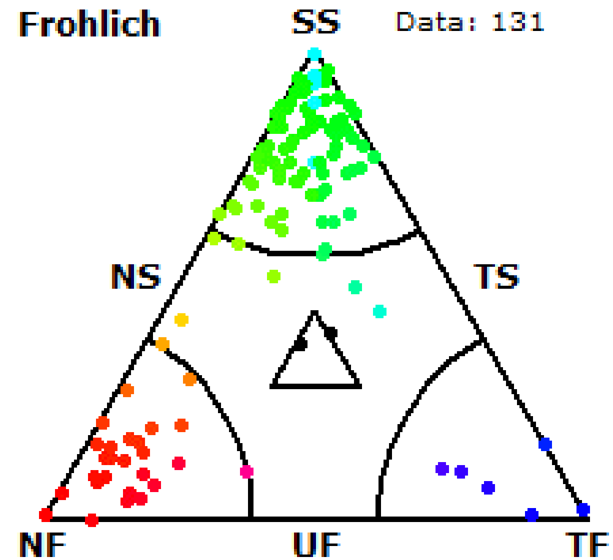

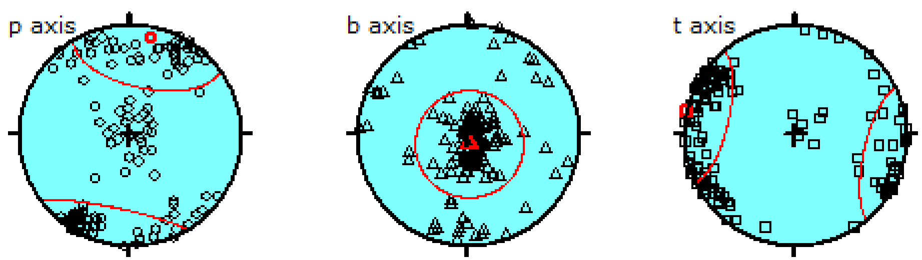

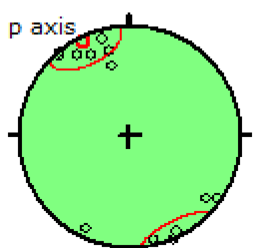

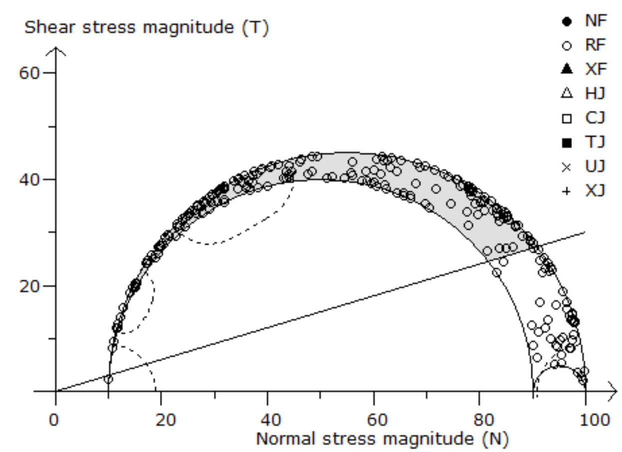

Región con mecanismos focales seleccionados para calcular estado de esfuerzos tectónicos LOCAL

Región MED SRTM 30 m

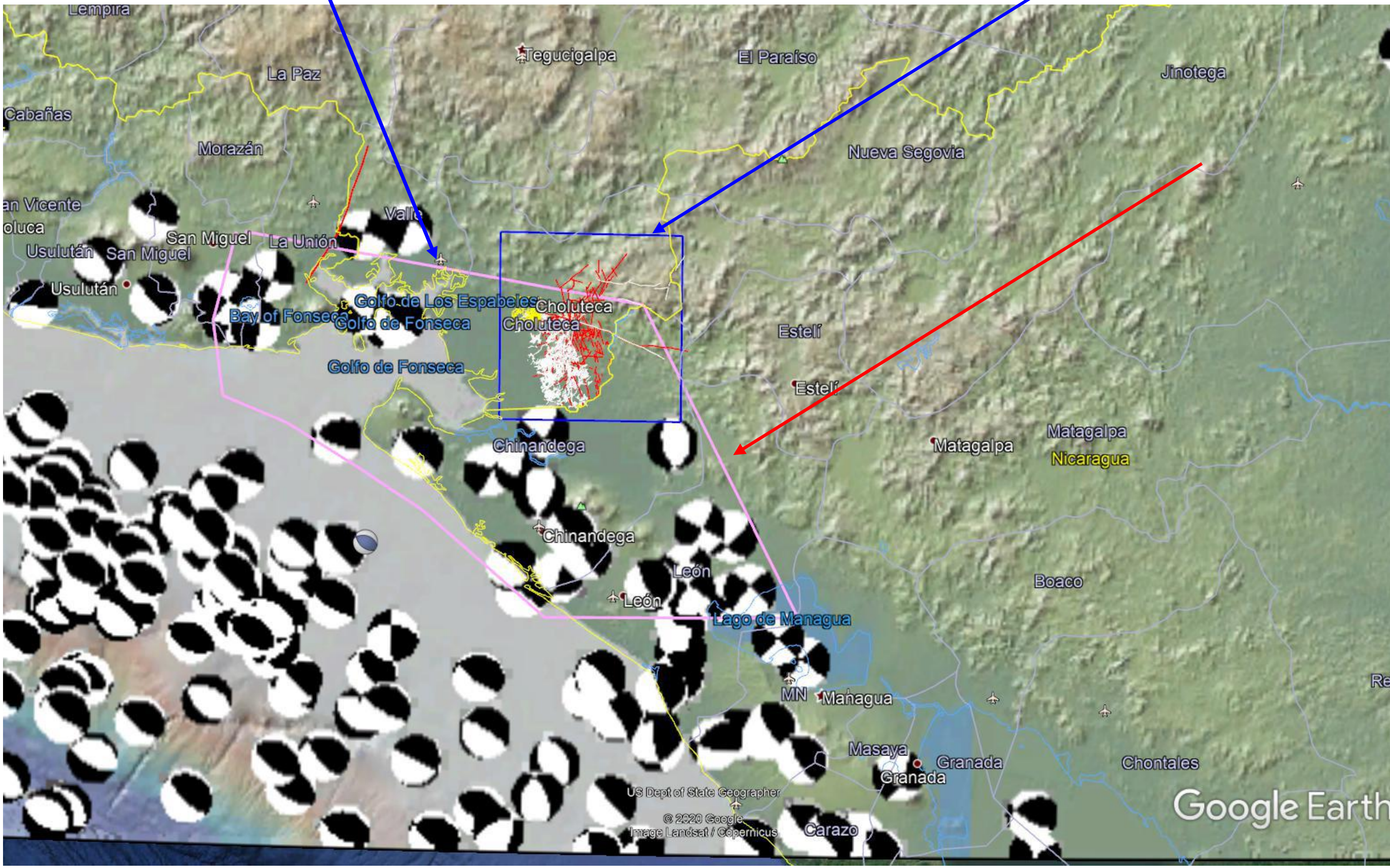

Se identifican y separan 2 estados de esfuerzos coexistentes
Con diferentes calidades y magnitudes no absolutas

STRIKE-SLIP al NW

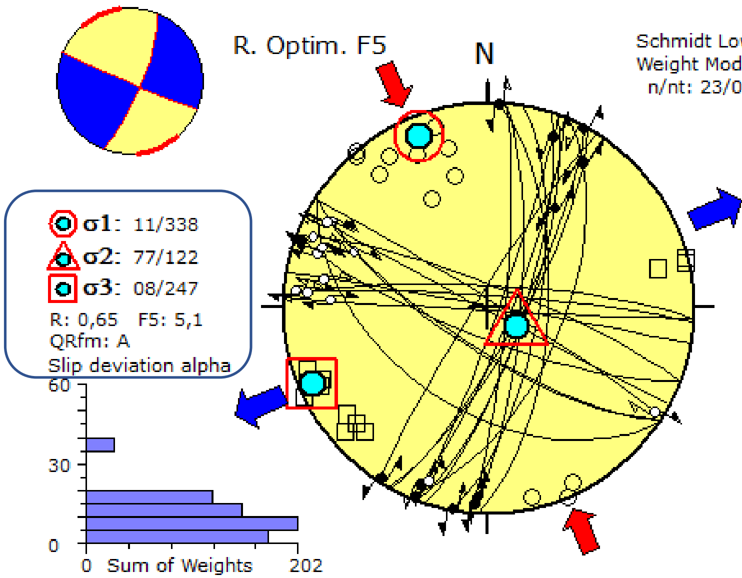

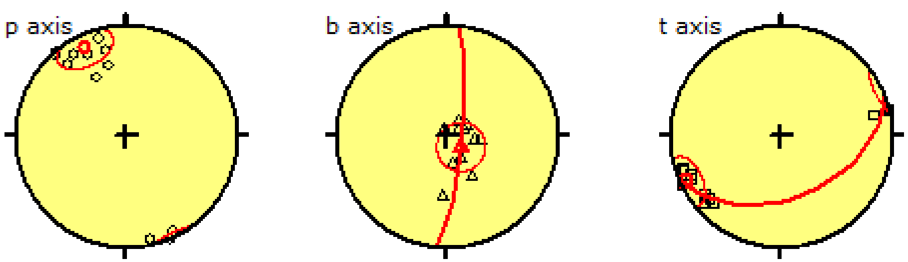

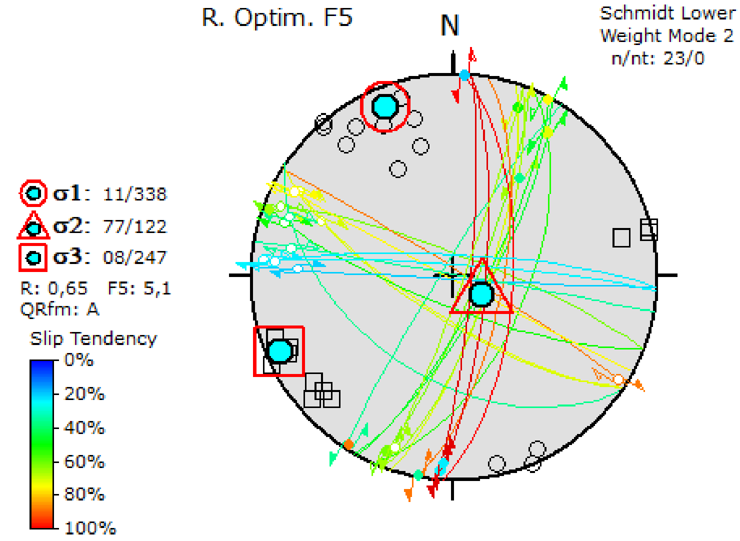

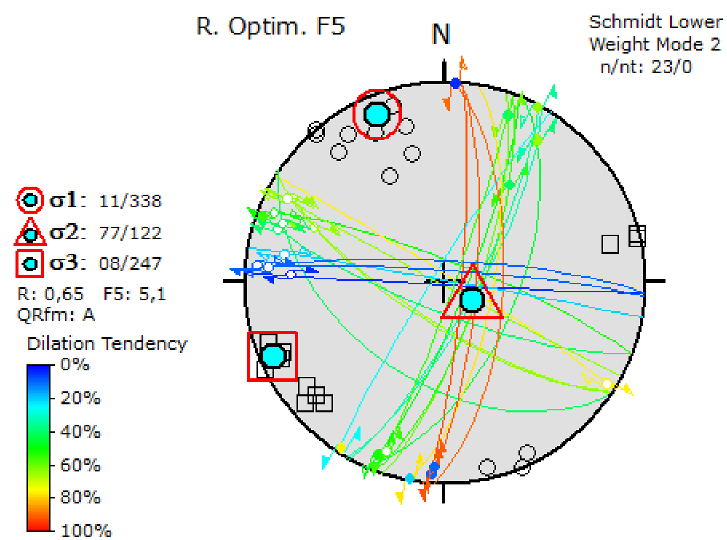

R’ = 1.03

STRIKE-SLIP al NWW,
menor calidad © y muy inestable

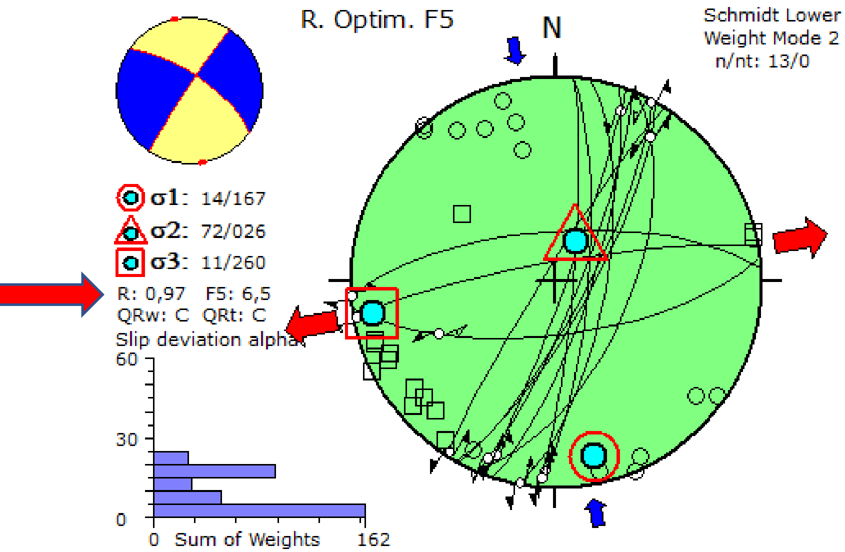

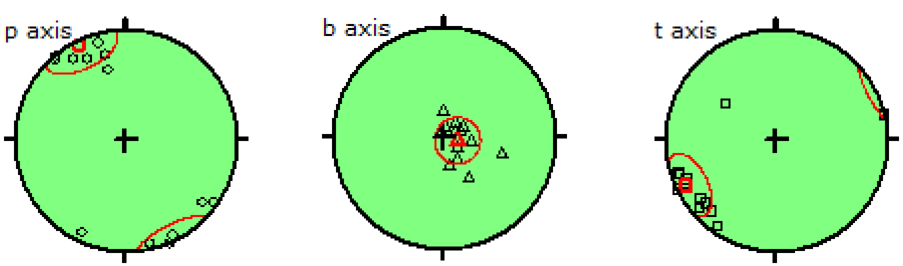

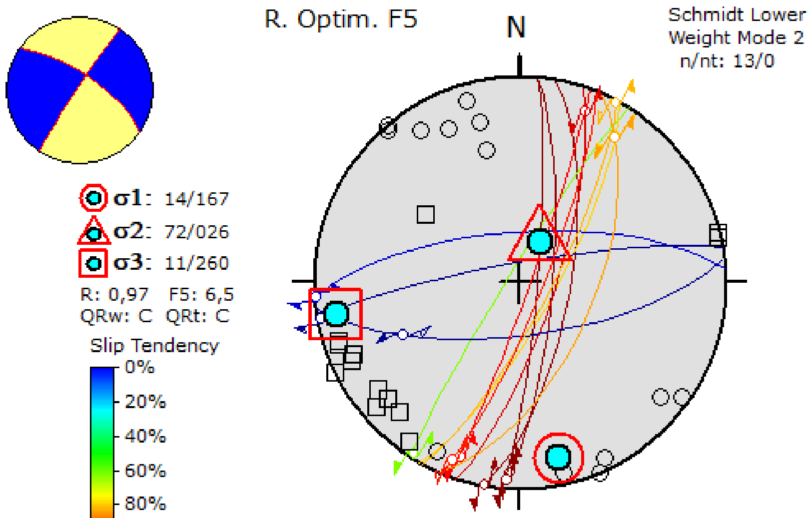

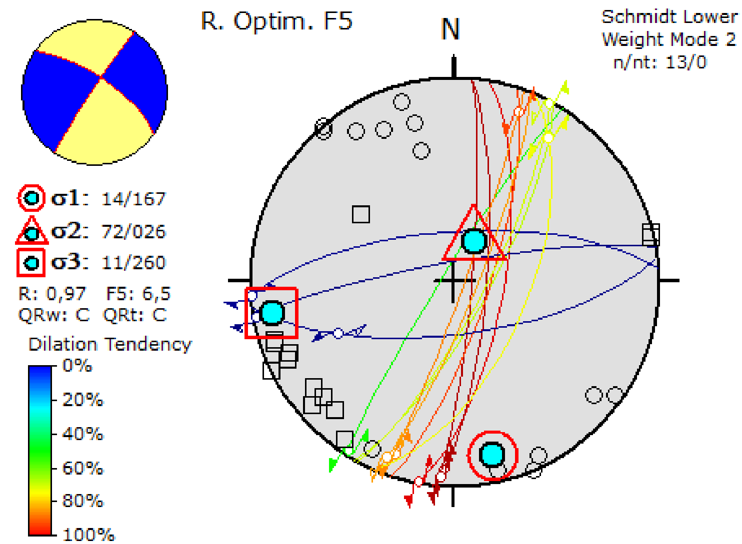

Esperaba un régimen compresivo
con fallas-mecanismos inversos
asociados a la subducción
(hasta los 25 Km de profundidad)

Se investigará el estado con
hipocentros a mayores
profundidades

Modelo Deformación Neotectónica y direcciones del ESFUERZO HORIZONTAL MÁXIMO. Allan López 1999.

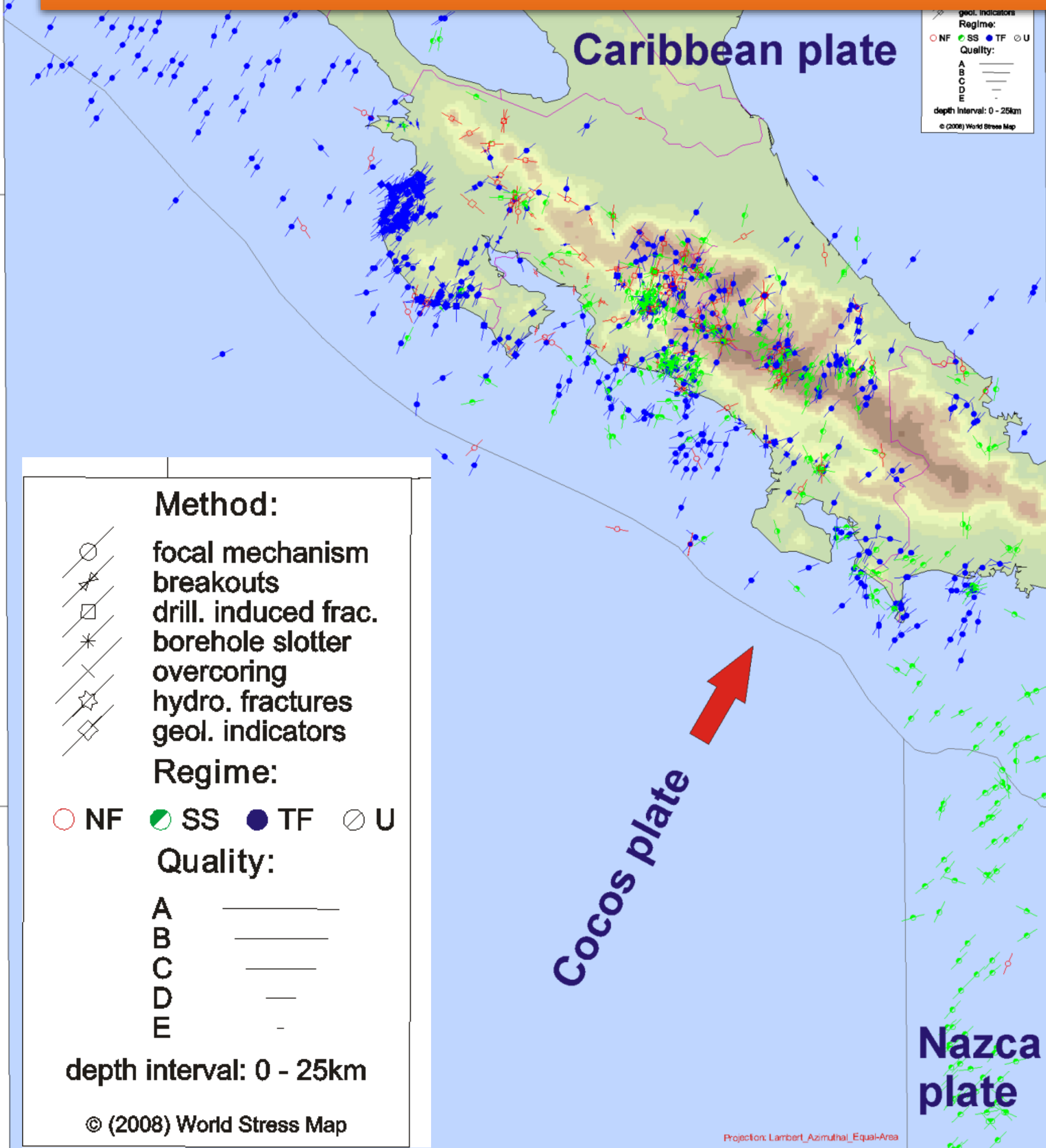

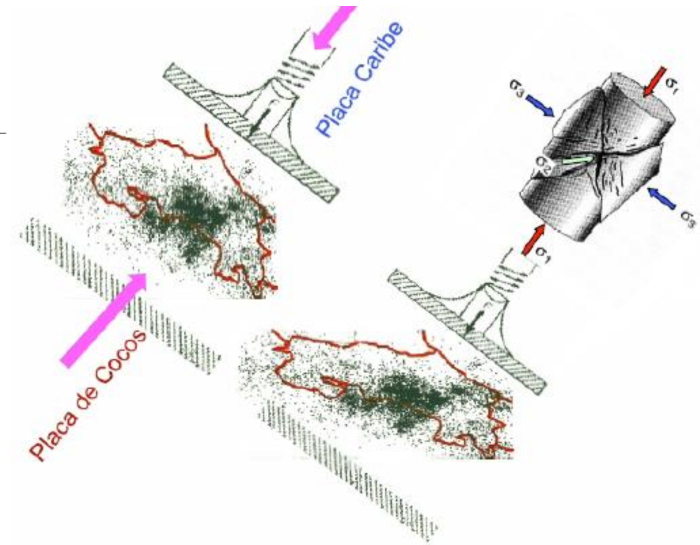

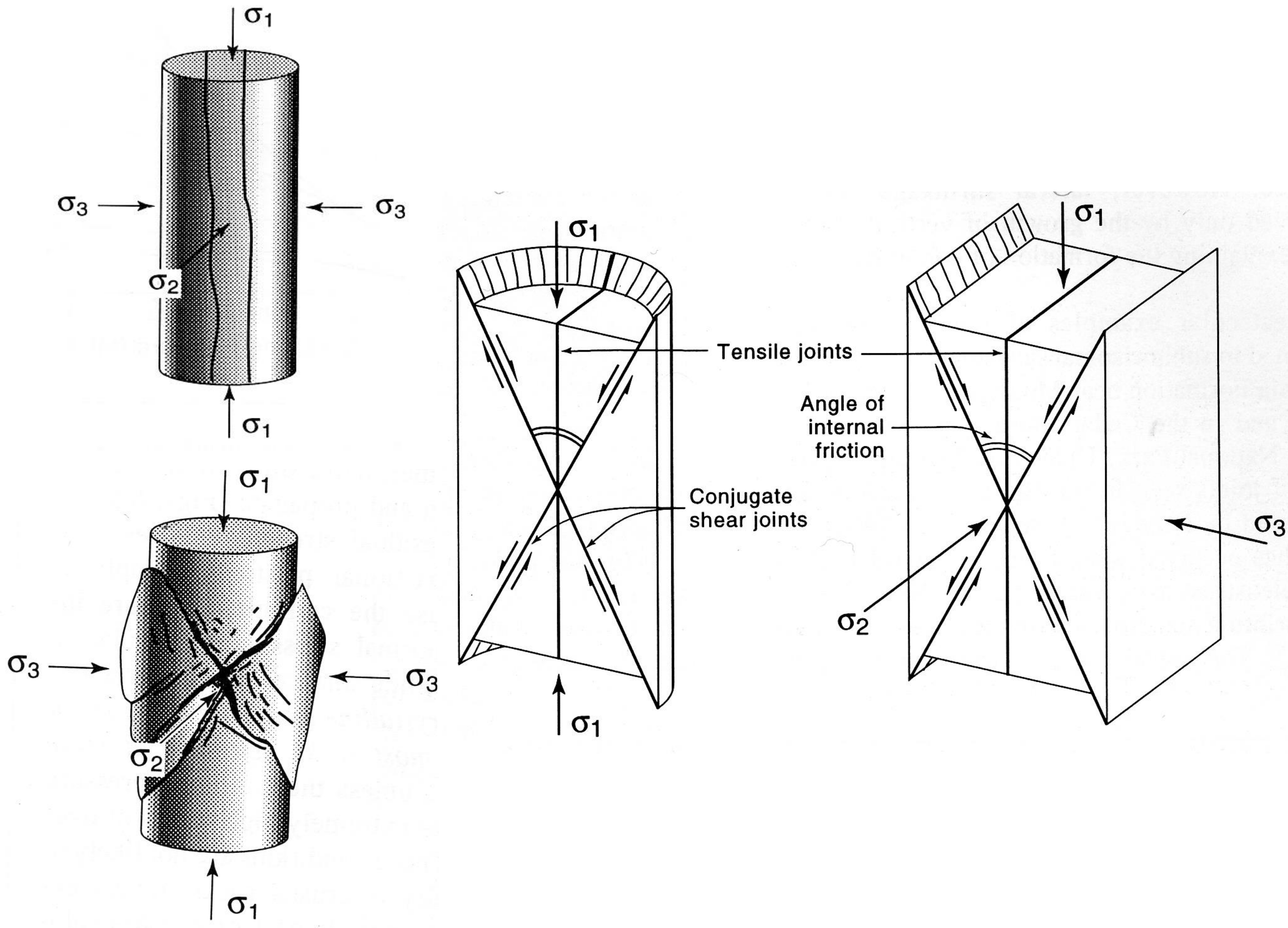

σ_1
σ_3
σ_3
σ_2
σ_1
σ_1
σ_3
σ_3
σ_2
σ_1
σ_1
Tensile joints
Conjugate shear joints
σ_1
σ_1
Angle of internal friction
σ_3
σ_2

Interpolación del **SH Max en rojo**.
Datos originales en negro

[***http://shine.rm.ingv.it/index.phtml***](http://shine.rm.ingv.it/index.phtml)

SHINE

1. Data selection:
Custom file

2. Geographical setting:
Longitude: -89.43°/-85.78°
Latitude: 11.95°/14.36°
Grid spacing: 0.1

3. Strategic parameters:
Searching radius: 2
Minimum cluster: 3
90% confidence bounds: 40°

2 Planos nodales de cada evento Mw > 4.0

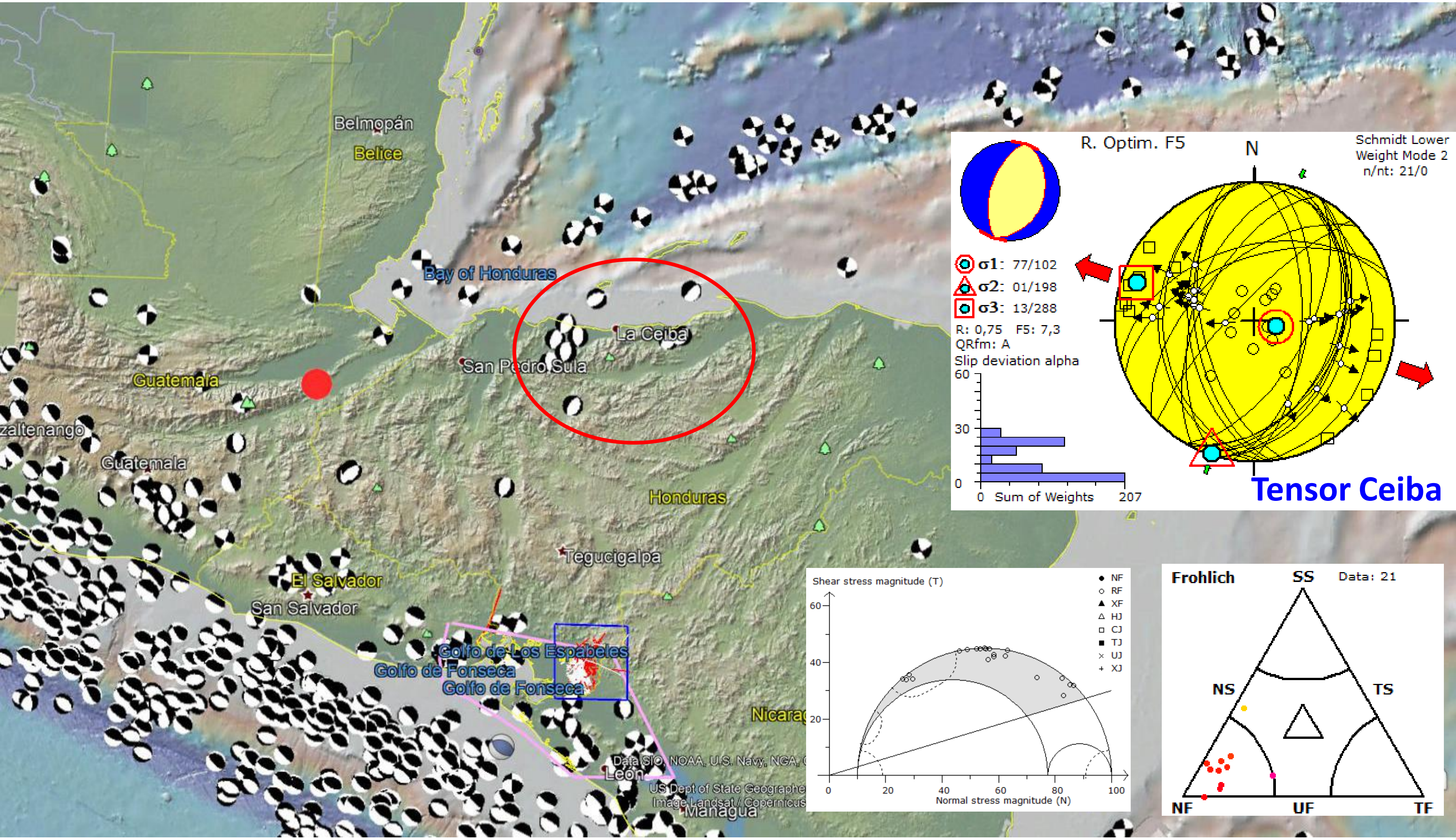

2 Planos nodales de cada evento Mw > 4.0

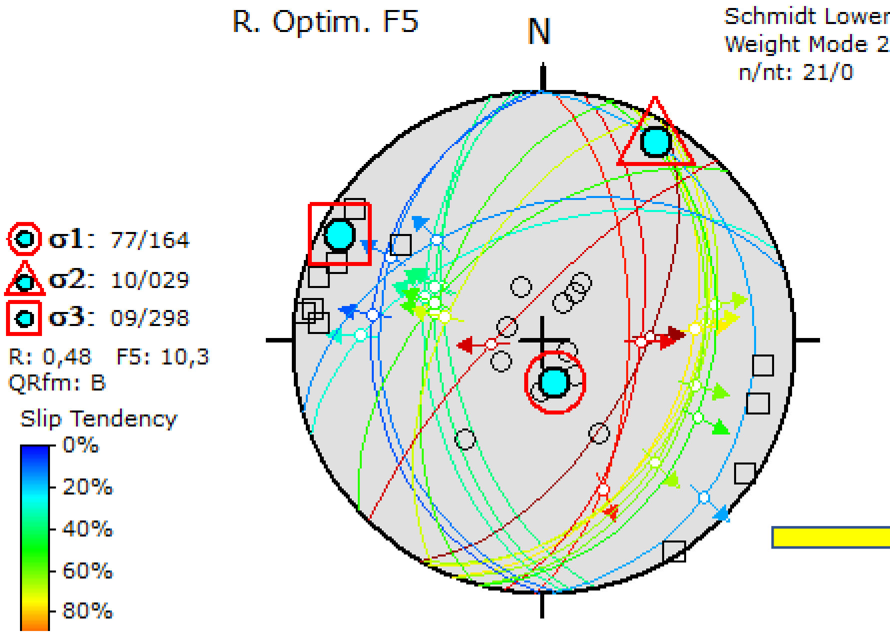

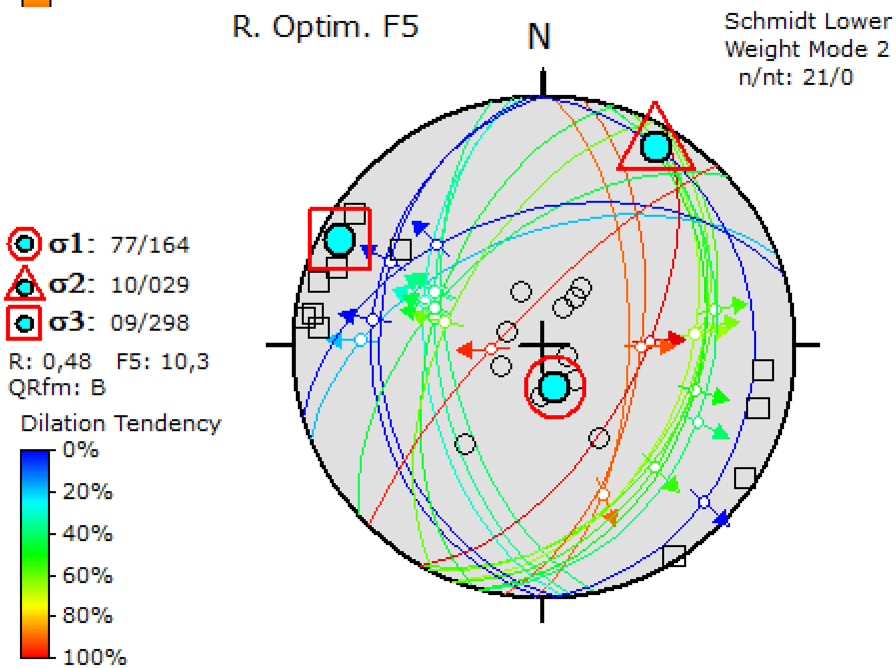

Tensor Ceiba

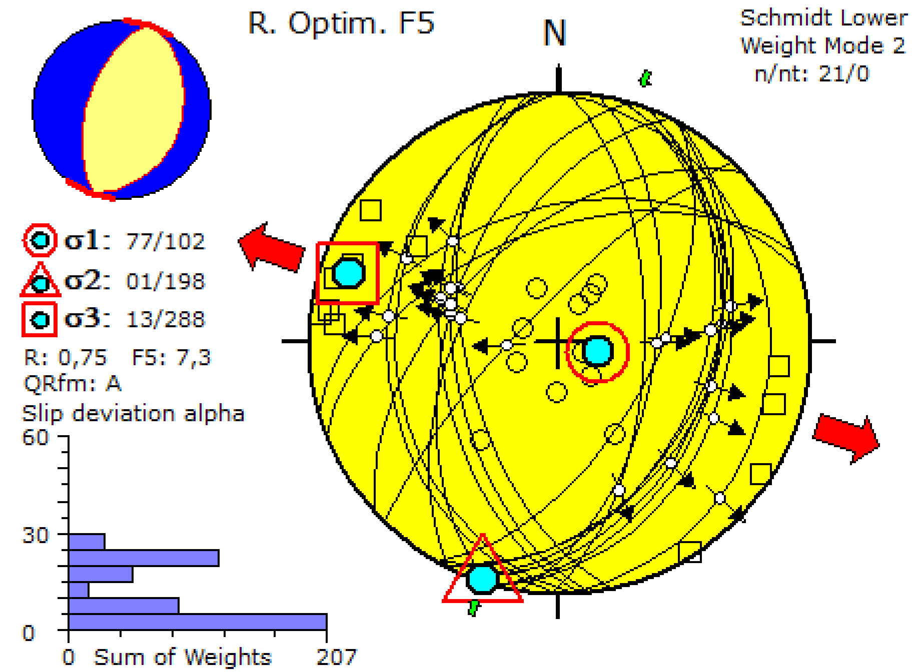

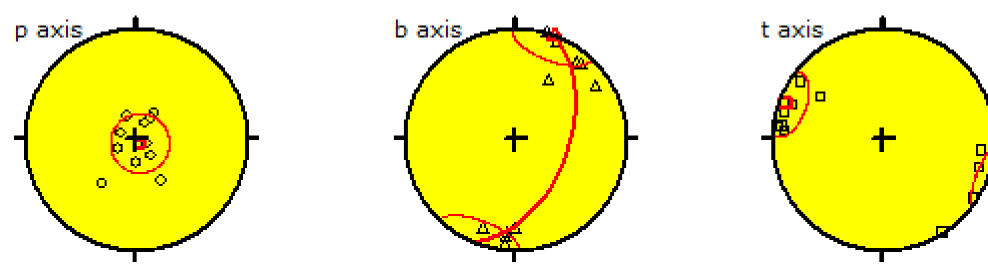

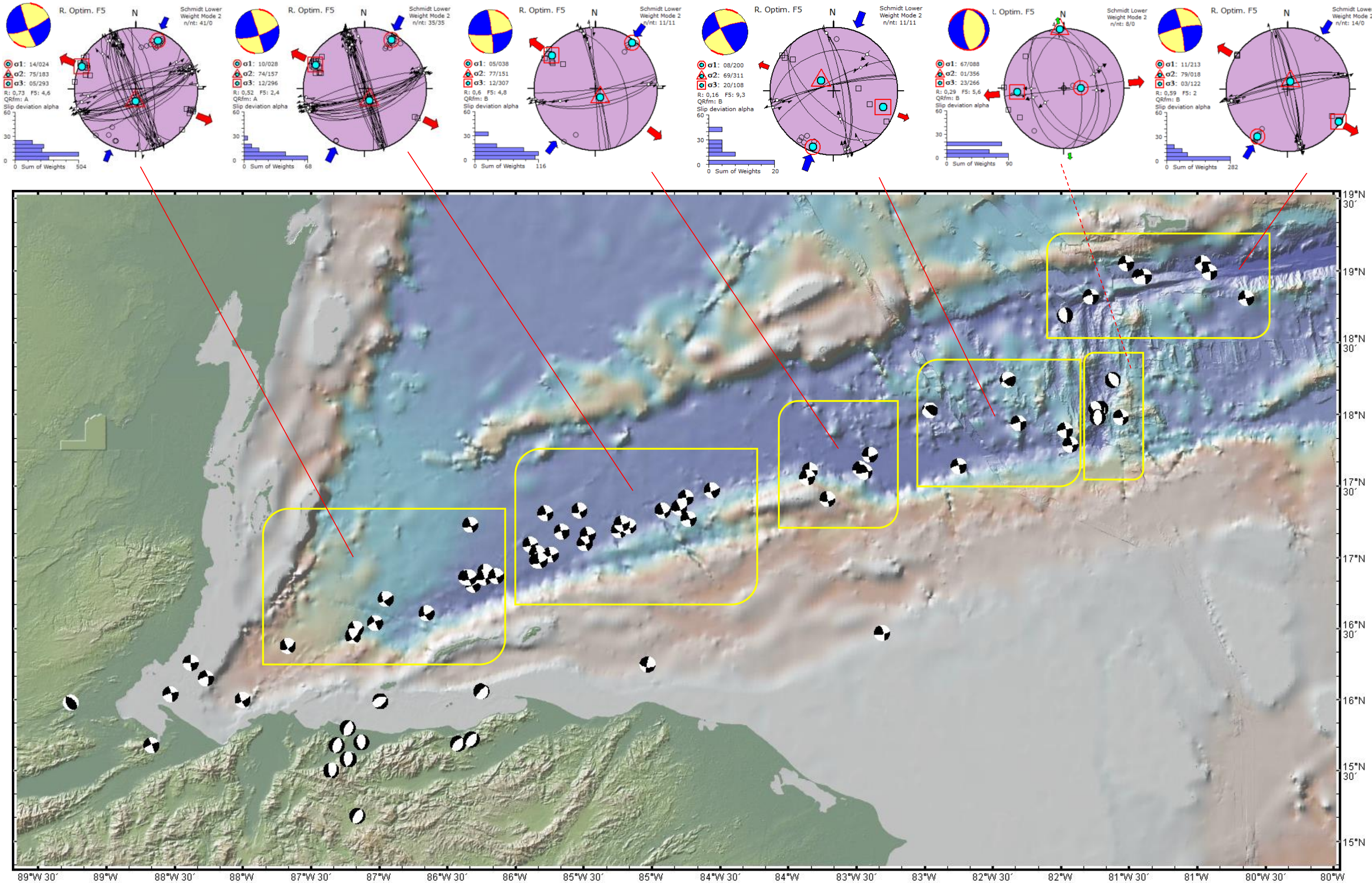
R. Optim. F5
Schmidt Lower
Weight Mode 2
n/nt: 41/0
σ1: 14/024
σ2: 75/183
σ3: 05/293
R: 0,73 F5: 4,6
QRfm: A
Slip deviation alpha
Sum of Weights 504
R. Optim. F5
Schmidt Lower
Weight Mode 2
n/nt: 35/35
σ1: 10/028
σ2: 74/157
σ3: 12/296
R: 0,52 F5: 2,4
QRfm: A
Slip deviation alpha
Sum of Weights 68
R. Optim. F5
Schmidt Lower
Weight Mode 2
n/nt: 11/11
σ1: 05/038
σ2: 77/151
σ3: 12/307
R: 0,6 F5: 4,8
QRfm: B
Slip deviation alpha
Sum of Weights 116
R. Optim. F5
Schmidt Lower
Weight Mode 2
n/nt: 11/11
σ1: 08/200
σ2: 69/311
σ3: 20/108
R: 0,16 F5: 9,3
QRfm: B
Slip deviation alpha
Sum of Weights 20
L. Optim. F5
Schmidt Lower
Weight Mode 2
n/nt: 8/0
σ1: 67/088
σ2: 01/356
σ3: 23/266
R: 0,29 F5: 5,6
QRfm: B
Slip deviation alpha
Sum of Weights 90
R. Optim. F5
Schmidt Lower
Weight Mode 2
n/nt: 14/0
σ1: 11/213
σ2: 79/018
σ3: 03/122
R: 0,59 F5: 2
QRfm: B
Slip deviation alpha
Sum of Weights 282
N
19°N 30′
19°N
18°N 30′
18°N
17°N 30′
17°N
16°N 30′
16°N
15°N 30′
15°N
89°W 30′
89°W
88°W 30′
88°W
87°W 30′
87°W
86°W 30′
86°W
85°W 30′
85°W
84°W 30′
84°W
83°W 30′
83°W
82°W 30′
82°W
81°W 30′
81°W
80°W 30′
80°W

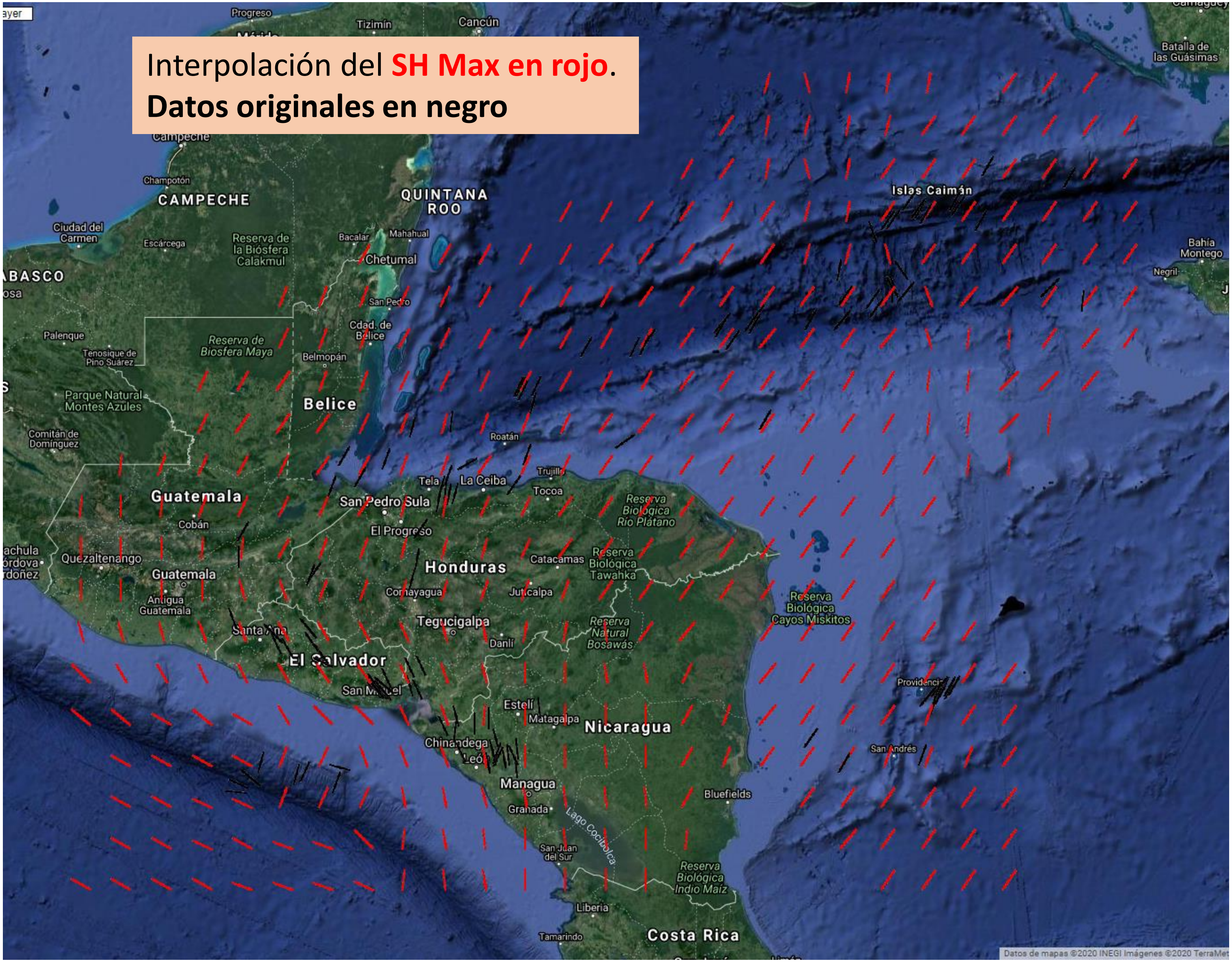
Interpolación del SH Max en rojo.
Datos originales en negro
Progreso
Tizimín
Cancún
Batalla de las Guásimas
Campeche
Champotón
CAMPECHE
QUINTANA ROO
Islas Caimán
Ciudad del Carmen
Escárcega
Reserva de la Biósfera Calakmul
Bacalar
Mahahual
Chetumal
Bahía Montego
Negril
San Pedro
Palenque
Cdad. de Belice
Reserva de Biosfera Maya
Belmopán
Tenosique de Pino Suárez
Parque Natural Montes Azules
Belice
Comitán de Domínguez
Roatán
Trujillo
Tela
La Ceiba
Tocoa
Guatemala
San Pedro Sula
Reserva Biológica Río Plátano
Cobán
El Progreso
Quezaltenango
Guatemala
Catacamas
Reserva Biológica Tawahka
Honduras
Comayagua
Juticalpa
Antigua Guatemala
Reserva Biológica Cayos Miskitos
Tegucigalpa
Reserva Natural Bosawás
Santa Ana
Danlí
El Salvador
Providencia
San Miguel
Estelí
Matagalpa
Nicaragua
Chinandega
San Andrés
Managua
Granada
Bluefields
Lago Cocibolca
San Juan del Sur
Reserva Biológica Indio Maíz
Liberia
Tamarindo
Costa Rica
Datos de mapas ©2020 INEGI Imágenes ©2020 TerraMet

Interpolación del **SH Max en rojo**.
Datos originales en negro y FALLAS

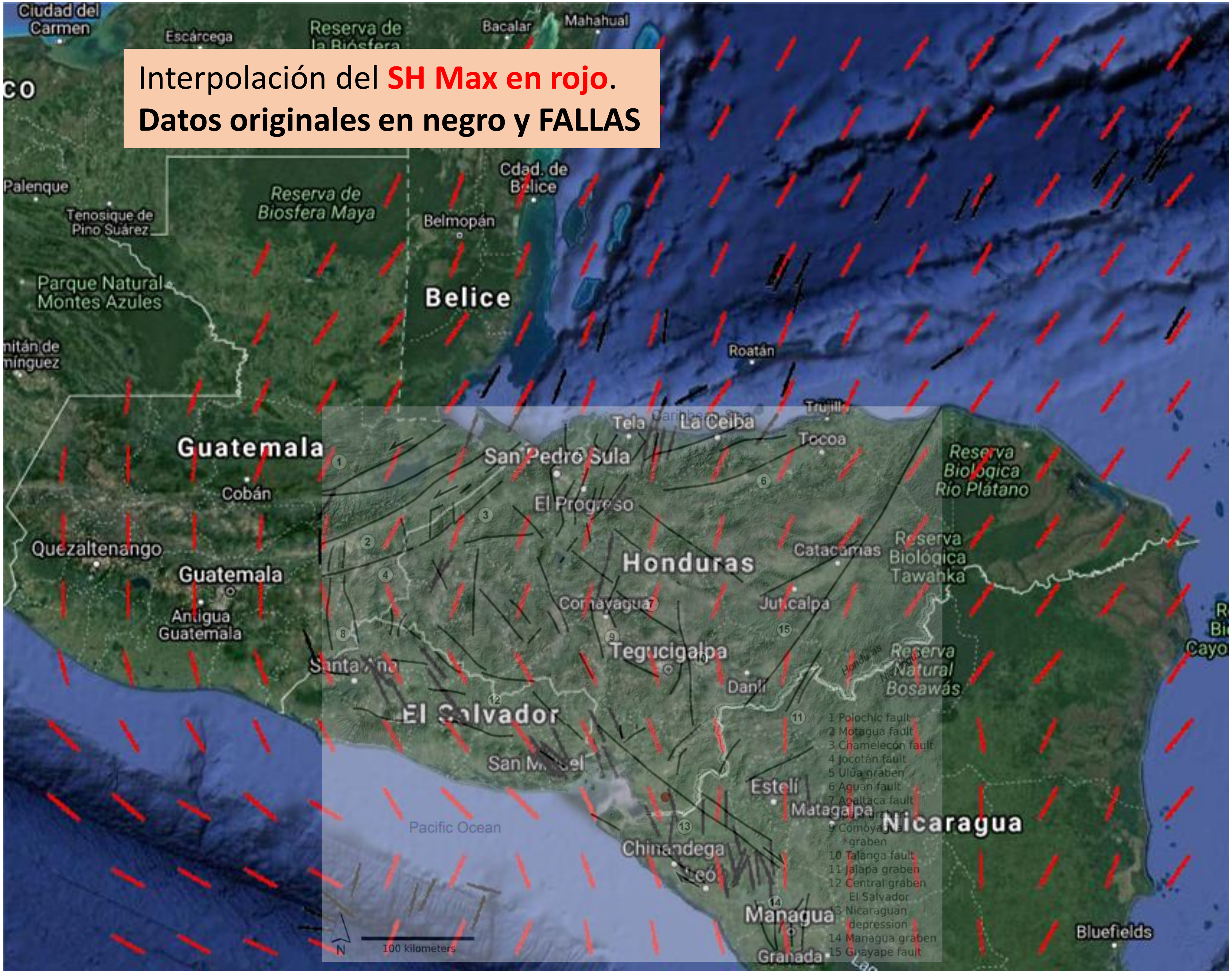

Interpolación del **SH Max en rojo**.

Datos originales en negro

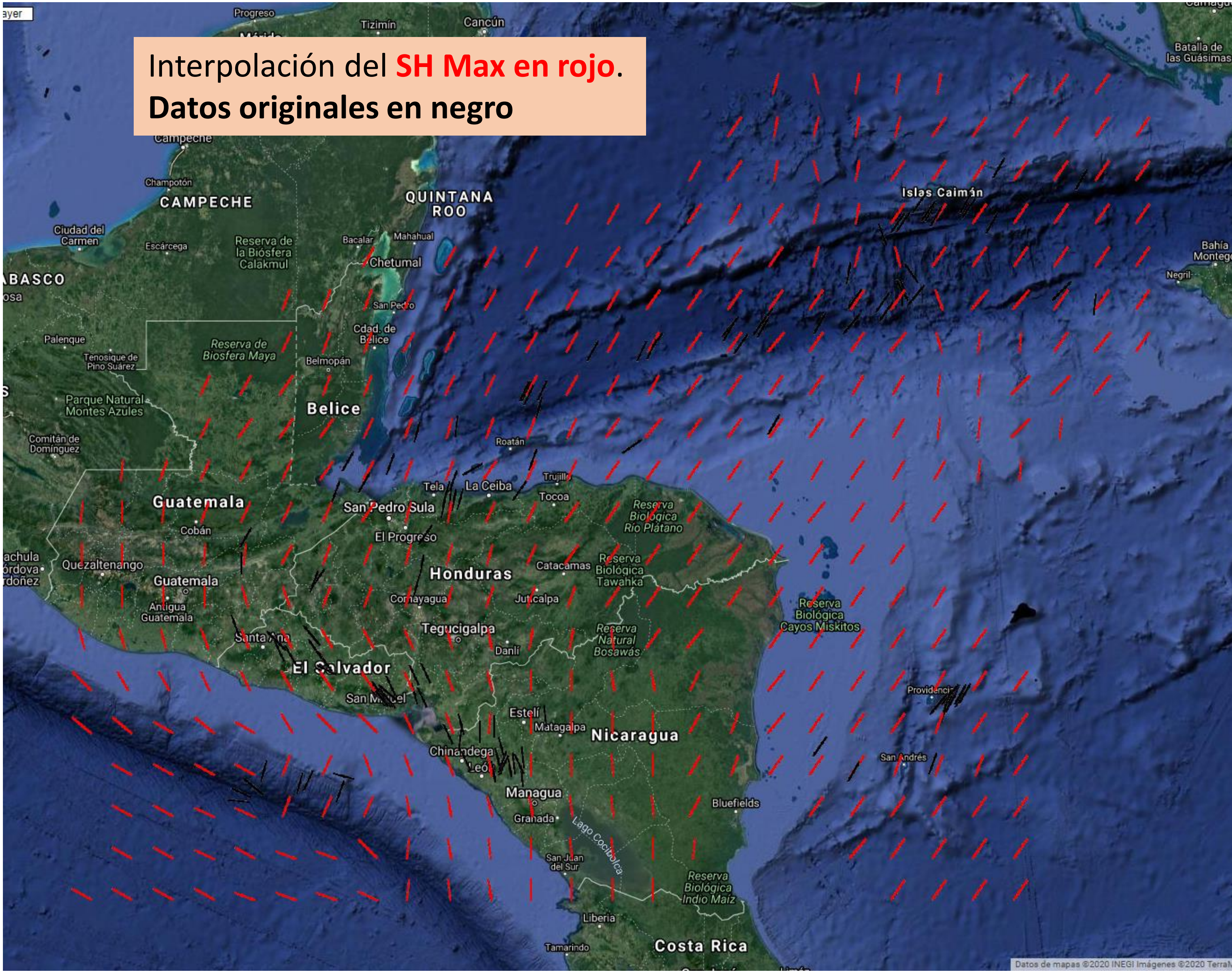

Interpolación del **SH Max en rojo**.
Datos originales en negro y FALLAS

Aplicaciones

Definitions for some reservoir petrophysical properties

derived from the acting stress tensor

ELSEVIER

Earth and Planetary Science Letters

Volume 478, 15 November 2017, Pages 159-174

Igneous sills record far-field and near-field stress interactions during volcano construction: Isle of Mull, Scotland

T.L. Stephens [a], R.J. Walker [a], D. Healy [b], A. Bubeck [a], R.W. England [a], K.J.W. McCaffrey [c]

⊞ Show more

https://doi.org/10.1016/j.epsl.2017.09.003

Slip and dilation tendency **show the attitude of planes susceptible to reactivation, via shear or dilation respectively.**

A plane is susceptible to slip when the ratio of shear stress (τ) to the normal stress acting on the plane (σn) is large. **Slip tendency** is normalised here (relative to the maximum possible slip tendency, Ts(max)) to enable comparison between stress states (Eq. (1); Morris et al., 1996):

(1) **Ts=(τ/σn)/Ts(max)**

A plane is susceptible to dilation when the difference between σ1 and the normal stress acting on the plane approaches the magnitude of differential stress (σD, where σD=σ1–σ3; Eq. (2); Ferrill et al., 1999):

$$T_d = \frac{(\sigma_1 - \sigma_\tau)}{(\sigma_1 - \sigma_3)}$$

Fracture susceptibility (Eq. (3); e.g. Mildren et al., 2002) represents the magnitude of fluid pressure change (ΔPf: either magmatic pressure within a crack, or hydrous pore-fluid pressure within a crack or the host rock pore space) that is required to cause shear reactivation.

Fluid-driven shear reactivation is dependent on the shear and normal stresses acting on the plane, as well as its cohesion (here assumed = 0), and static coefficient of friction (μs):

$$S_f = \sigma_n - (\tau / \mu_s) \quad (3)$$

Reactivation via fluid-driven dilation would require a fluid pressure greater than the fracture susceptibility.

Intrusion is favoured where Td is high and fracture susceptibility is low.

Shear reactivation is favoured where Ts is high and fracture susceptibility is low.

The ***opening angle*** is related to the

shear stress (τ),
normal stress (σ_n), and
fluid pressure (P_f)

$$\mu = \tan^{-1}\left(\frac{\tau}{P_f - \sigma_n}\right)$$

acting on that plane at the time of intrusion (Delaney et al., 1986; Jolly and Sanderson,
1997):

Equation (5) shows that if the fluid overpressure ($P_f - \sigma_n$) is equal to the shear stress, the opening angle is 45°, and the shear-to-dilation ratio is unity. If the overpressure is greater than the shear stress, the opening angle is less than 45°, and the fracture will show a greater component of dilation to shear.

When μ is negative, the fracture will remain closed as the fluid pressure did not exceed the normal stress.

An intrusive segment, however, may inflate against a closed fracture (where $P_f < \sigma_n$), causing a local contractional shear and a blunt intrusion tip.

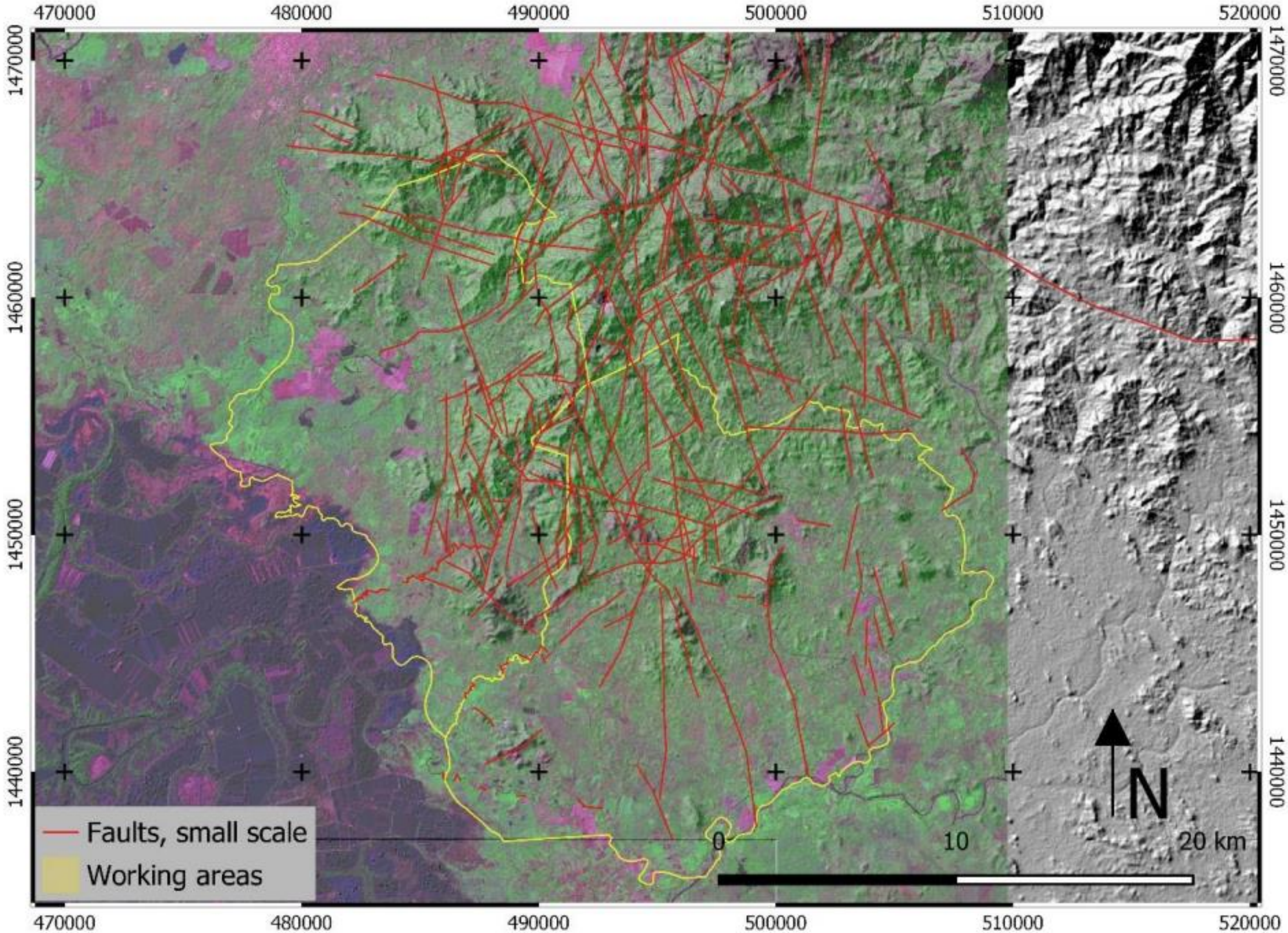

Figure 5.4: Lineaments interpreted as faults of the working areas and the surrounding areas in a small scale. Sentinel 2A, bands 12, 8a, 5 (RGB) over shaded relief SRTM DEM.

Lineamientos identificados por BGR, 2019 en Namasigüe-El Triunfo

(Alina Ermertz & Dr. Kai Hahne)

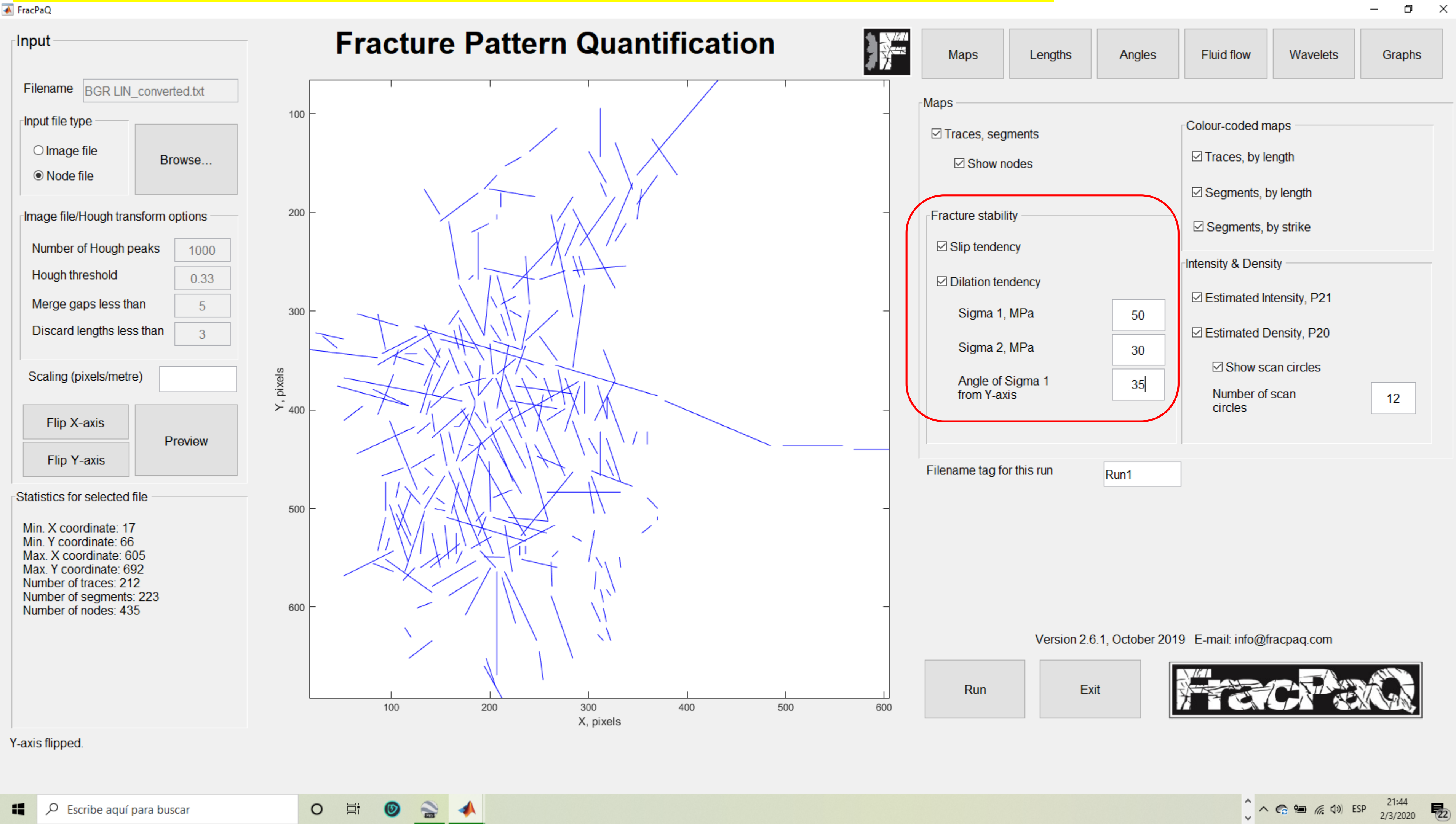

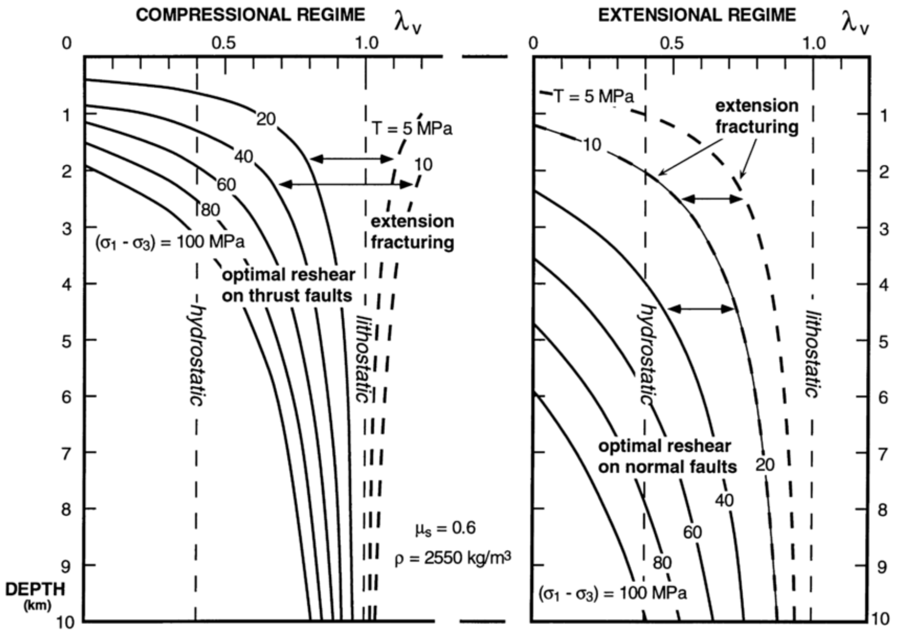

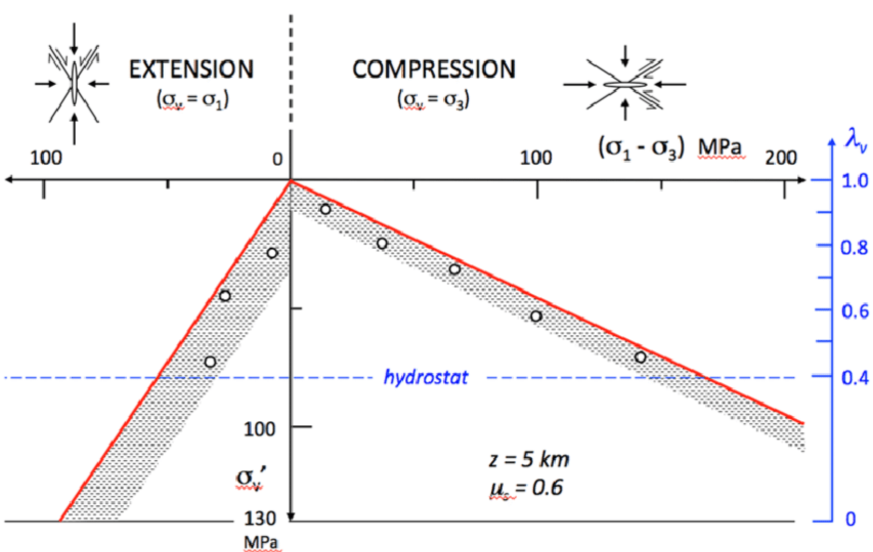

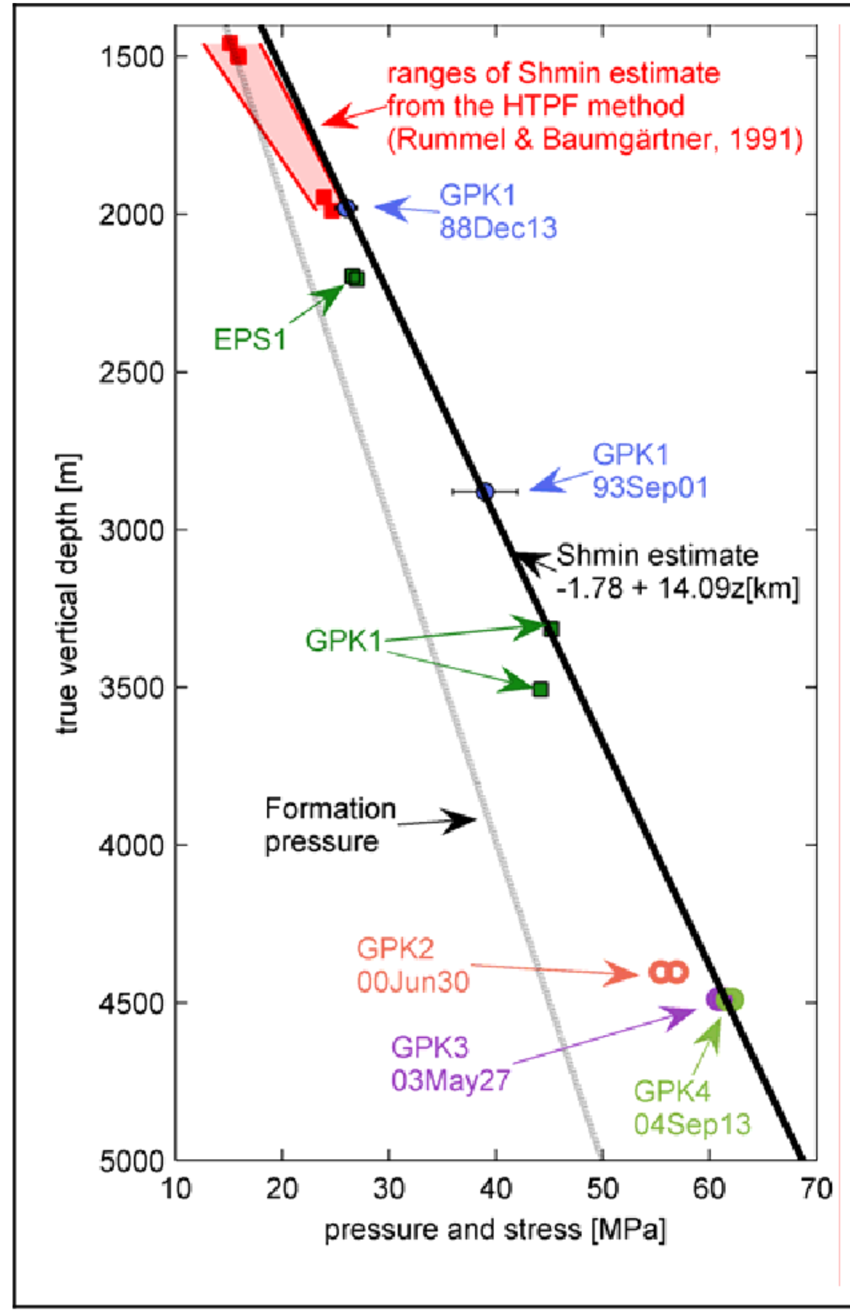

Figure 4: Estimates of the Shmin from small-volume

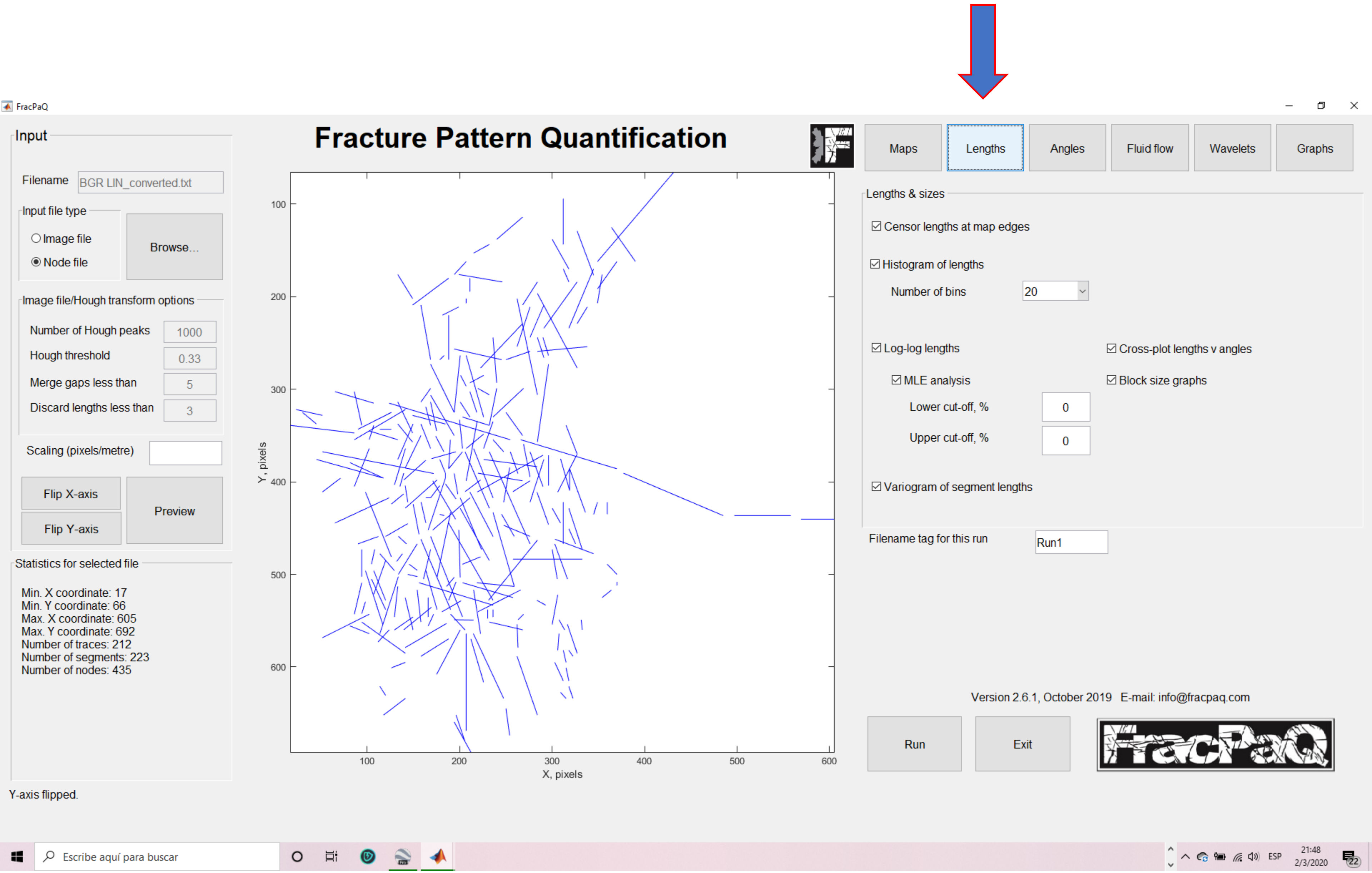
FracPaQ
Input
Fracture Pattern Quantification
Maps
Lengths
Angles
Fluid flow
Wavelets
Graphs
Filename
BGR LIN_converted.txt
Input file type
Image file
Node file
Browse...
Image file/Hough transform options
Number of Hough peaks
1000
Hough threshold
0.33
Merge gaps less than
5
Discard lengths less than
3
Scaling (pixels/metre)
Flip X-axis
Flip Y-axis
Preview
Statistics for selected file
Min. X coordinate: 17
Min. Y coordinate: 66
Max. X coordinate: 605
Max. Y coordinate: 692
Number of traces: 212
Number of segments: 223
Number of nodes: 435
Y-axis flipped.
Y, pixels
X, pixels
Lengths & sizes
Censor lengths at map edges
Histogram of lengths
Number of bins
20
Log-log lengths
Cross-plot lengths v angles
MLE analysis
Block size graphs
Lower cut-off, %
0
Upper cut-off, %
0
Variogram of segment lengths
Filename tag for this run
Run1
Version 2.6.1, October 2019 E-mail: info@fracpaq.com
Run
Exit
FracPaQ
Escribe aquí para buscar
ESP
21:48
2/3/2020

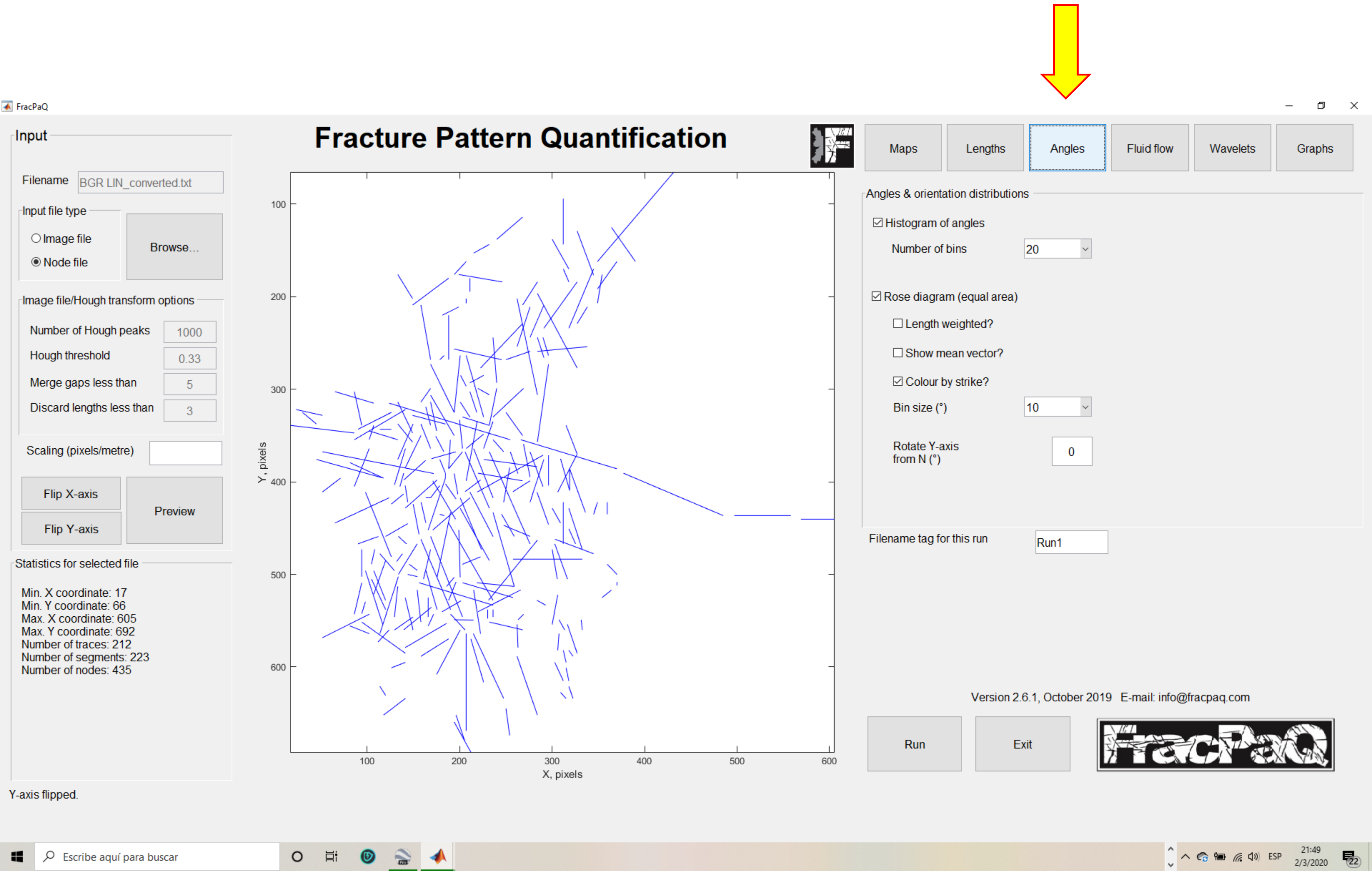
FracPaQ
Fracture Pattern Quantification
Input
Filename
BGR LIN_converted.txt
Input file type
Image file
Node file
Browse...
Image file/Hough transform options
Number of Hough peaks
1000
Hough threshold
0.33
Merge gaps less than
5
Discard lengths less than
3
Scaling (pixels/metre)
Flip X-axis
Flip Y-axis
Preview
Statistics for selected file
Min. X coordinate: 17
Min. Y coordinate: 66
Max. X coordinate: 605
Max. Y coordinate: 692
Number of traces: 212
Number of segments: 223
Number of nodes: 435
Y-axis flipped.
Y, pixels
X, pixels
Maps
Lengths
Angles
Fluid flow
Wavelets
Graphs
Angles & orientation distributions
Histogram of angles
Number of bins
20
Rose diagram (equal area)
Length weighted?
Show mean vector?
Colour by strike?
Bin size (°)
10
Rotate Y-axis from N (°)
0
Filename tag for this run
Run1
Version 2.6.1, October 2019 E-mail: info@fracpaq.com
Run
Exit
FracPaQ
Escribe aquí para buscar
ESP
21:49
2/3/2020

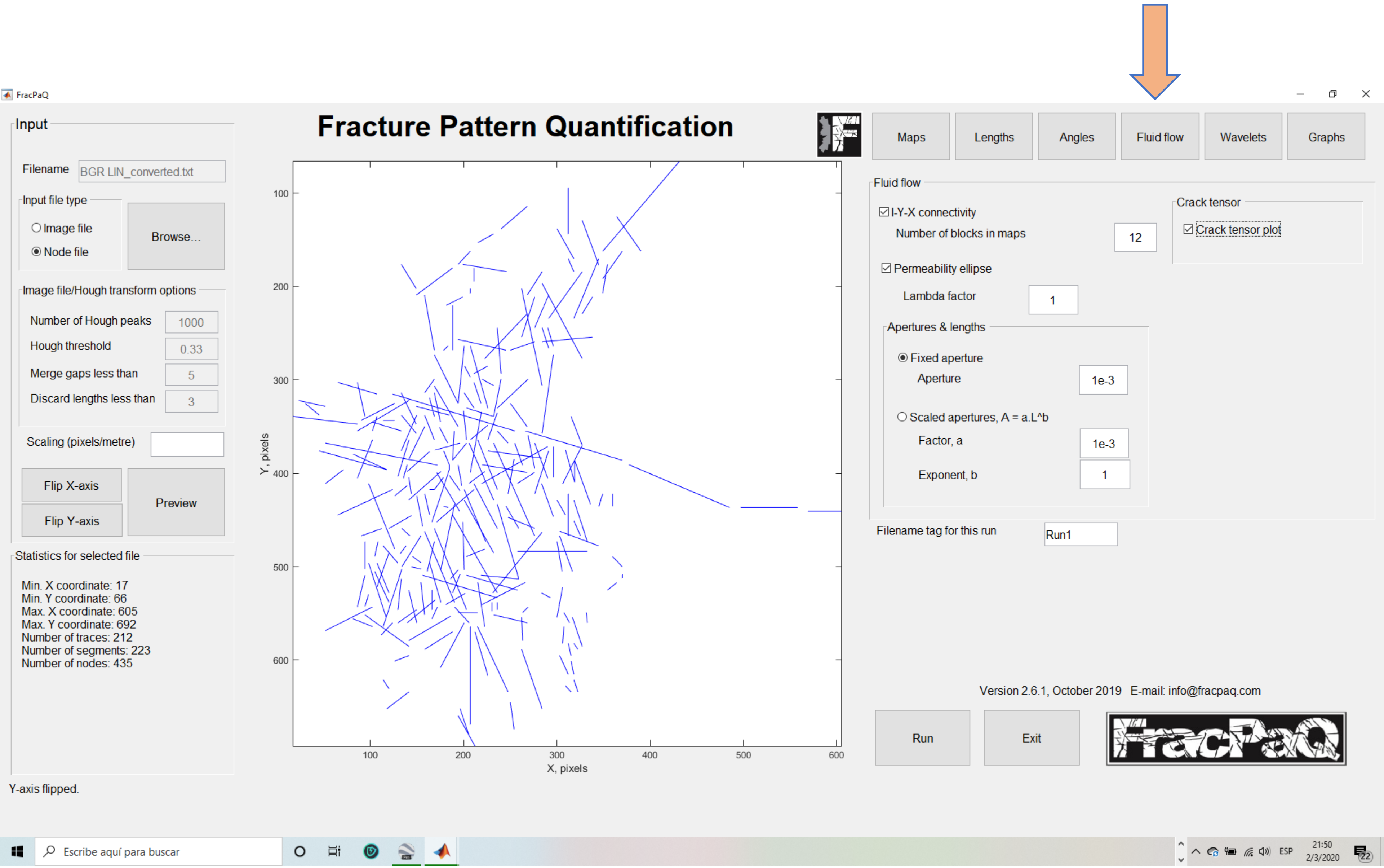
FracPaQ
Fracture Pattern Quantification
Input
Filename
BGR LIN_converted.txt
Input file type
Image file
Node file
Browse...
Image file/Hough transform options
Number of Hough peaks
1000
Hough threshold
0.33
Merge gaps less than
5
Discard lengths less than
3
Scaling (pixels/metre)
Flip X-axis
Flip Y-axis
Preview
Statistics for selected file
Min. X coordinate: 17
Min. Y coordinate: 66
Max. X coordinate: 605
Max. Y coordinate: 692
Number of traces: 212
Number of segments: 223
Number of nodes: 435
Y-axis flipped.
Y, pixels
X, pixels
Maps
Lengths
Angles
Fluid flow
Wavelets
Graphs
Fluid flow
I-Y-X connectivity
Number of blocks in maps
12
Permeability ellipse
Lambda factor
1
Apertures & lengths
Fixed aperture
Aperture
1e-3
Scaled apertures, A = a.L^b
Factor, a
1e-3
Exponent, b
1
Crack tensor
Crack tensor plot
Filename tag for this run
Run1
Version 2.6.1, October 2019 E-mail: info@fracpaq.com
Run
Exit
FracPaQ
Escribe aquí para buscar
ESP
21:50
2/3/2020

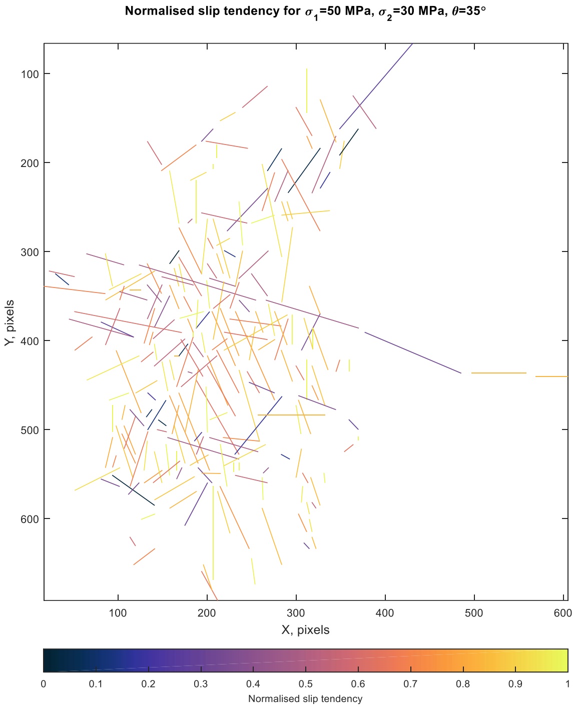

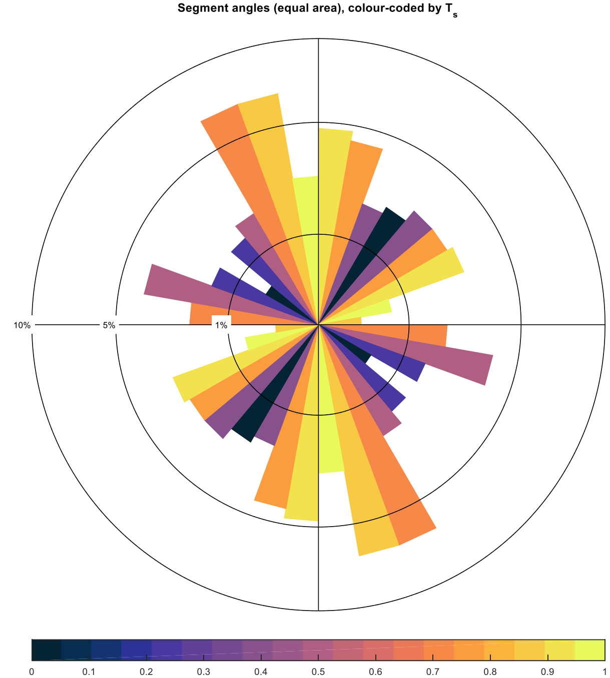

Ts=(τ/σn)/Ts(max)

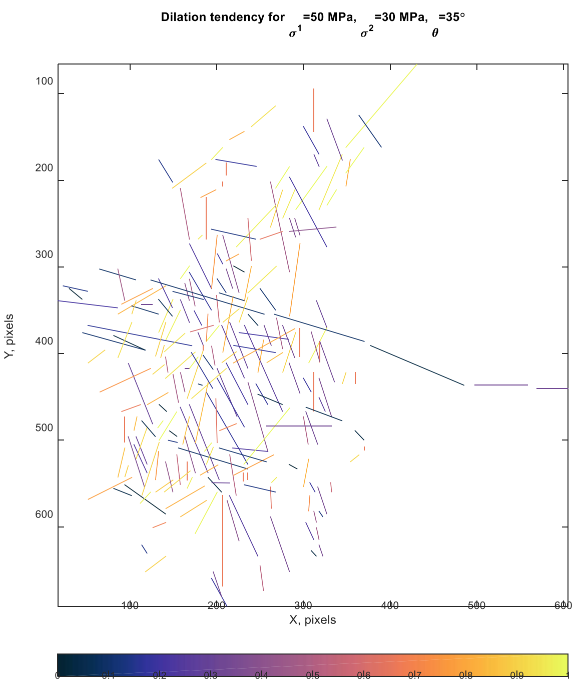

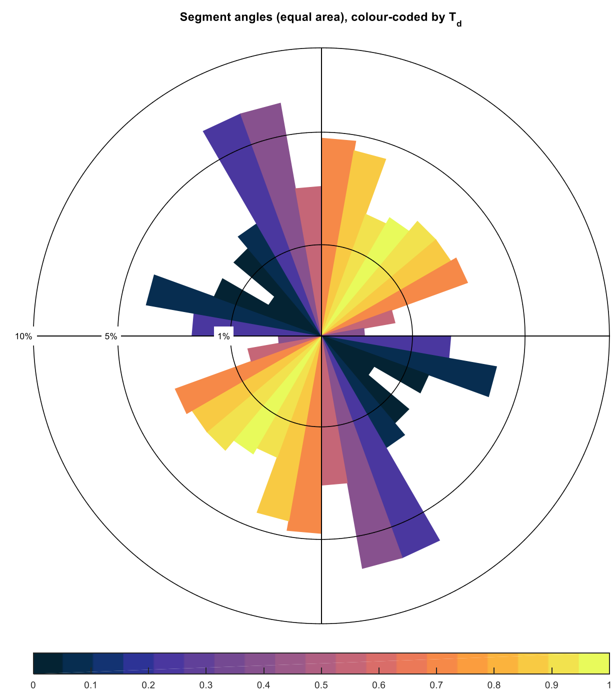

$$T_d = \frac{(\sigma_1 - \sigma_\tau)}{(\sigma_1 - \sigma_3)}$$

2 Planos nodales de cada evento Mw > 4.0

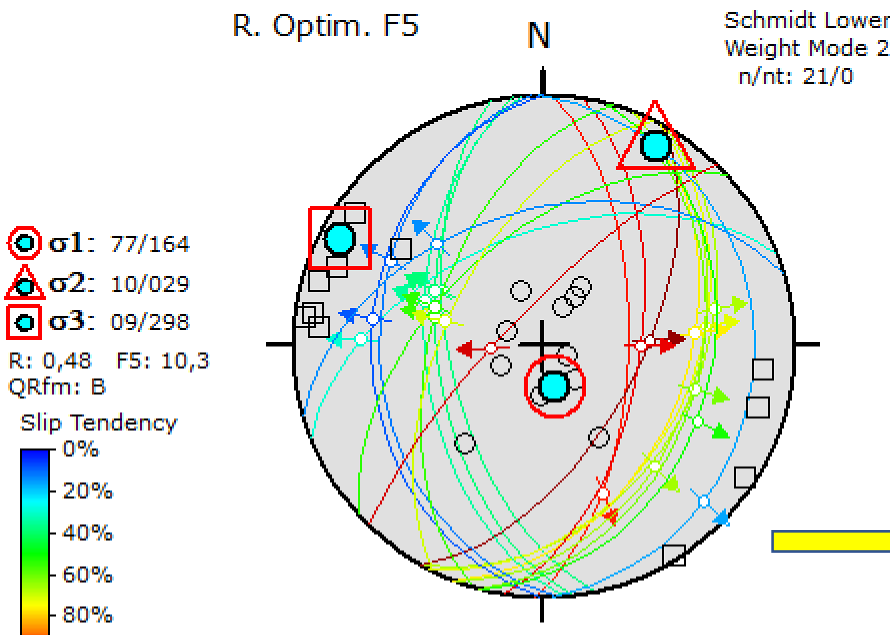

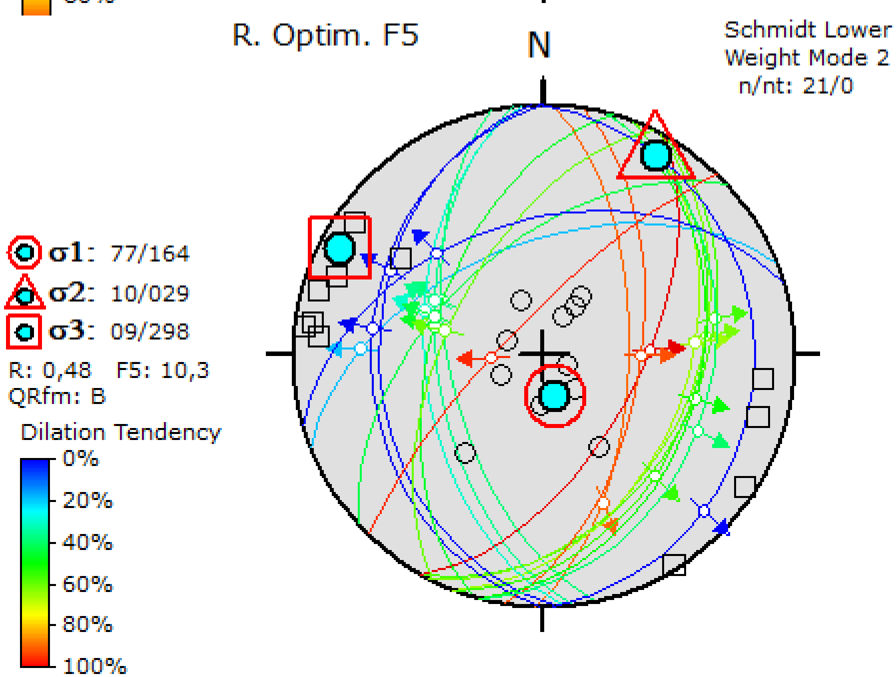

Tensor Ceiba

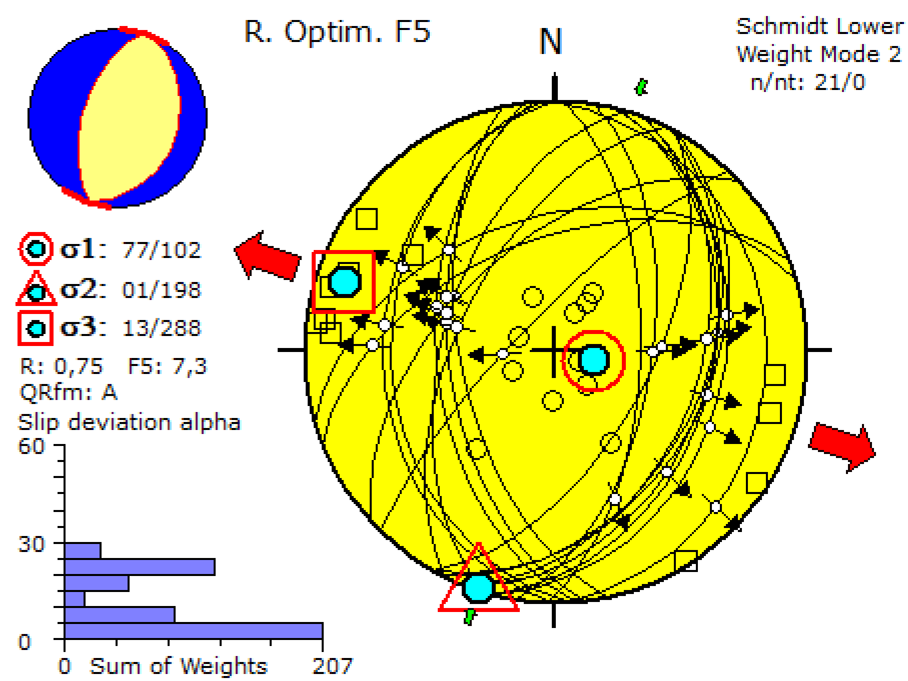

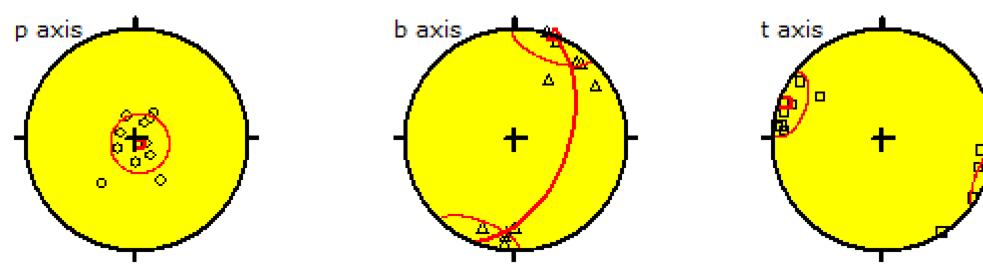

Muchas gracias por su paciencia

Preguntas ?

Dudas ?

Sospechas ?